

**ENERGY PERFORMANCE OF  
UNDERFLOOR AIR DISTRIBUTION (UFAD) SYSTEMS  
PART IV: UNDERFLOOR PLENUM TESTING AND MODELING**

**Fred Bauman and Hui Jin  
Center for the Built Environment**

**Commission Project Manager: Norman Bourassa  
PIER Buildings Program  
CEC Contract 500-01-035**

## **I INTRODUCTION**

---

This section provides full details of work performed in support of Task 2.3 (Underfloor Plenum Testing) and Task 2.5 (Underfloor Plenum Model Development). The ultimate goal of these tasks was to develop a model capable of calculating the thermal performance of underfloor air supply plenums, while at the same time suitable for implementation in EnergyPlus. A secondary goal was to conduct fundamental research that provides a sound theoretical and practical understanding of underfloor plenum energy performance in terms of heat transfer entering the plenum and the resulting airflow and temperature distributions. The technical approach used to accomplish this work included the following tasks:

- Full-scale experiments in CBE's underfloor plenum test facility
- Development of computational fluid dynamics (CFD) model of underfloor plenum
- Validation of CFD plenum model by comparison with full-scale experimental database
- Use of the validated CFD plenum model to conduct simulations of a broader range of plenum design and operational parameters
- Development of simplified underfloor plenum model based on CFD database for implementation into EnergyPlus
- Comparison between EnergyPlus and CFD plenum model predictions
- Simplified heat balance modeling study of heat transfer pathways in UFAD systems

## **2 TESTING AND CFD MODELING OF UNDERFLOOR AIR SUPPLY PLENUMS**

---

In this section we describe the development and validation of a computational fluid dynamics (CFD) model for predicting the airflow and thermal performance of underfloor air supply plenums. To provide validation data for comparison with the CFD model, a series of experiments in a full-scale underfloor plenum test facility were carried out. The results of the experiments and comparison with the model predictions are described for the major variables, including plenum airflow patterns and velocities, plenum air temperature distributions, and heat exchange between the exposed concrete slab, the underside of the raised floor panels, and the supply air as it flows through the plenum. The content of this section is taken largely from Jin et al. (2006). A more detailed description of this work with additional experimental and CFD results is contained in Jin et al. (2005).

## 2.1 INTRODUCTION

Underfloor air distribution (UFAD) offers several potential advantages over conventional overhead systems. However, barriers exist to widespread adoption of UFAD technology since it is a relatively new and unfamiliar technology. One of the major technical challenges is to precisely quantify the air movement and heat transfer behavior taking place in the underfloor air supply plenum. Cool supply air flowing through the underfloor plenum in a multi-story building is exposed to heat gain from both the concrete slab (conducted from the warm return air on the adjacent floor below the slab) and the raised floor panels (conducted from the warmer room above). The magnitude of this heat gain can be quite high, resulting in undesirable loss of control of the supply air temperature from the plenum into the occupied space, sometimes referred to as thermal decay (Bauman 2003). To date, evidence from completed projects indicates that excessive thermal decay can be a problem.

Due to the large number of possible plenum configurations (size, shape, number and location of plenum inlets, etc.) encountered in practice, along with the complexity of the airflow and thermal behavior, it is desirable to develop a validated mathematical model of underfloor air supply plenums. This has been the major objective of the research work described below. To characterize the major variables that must be accommodated by the underfloor plenum model, experiments were carried out in a full-scale underfloor plenum test facility. A range of practical design and operating parameters that can affect the performance of UFAD systems has been investigated. The fundamental heat transfer processes and parameters that have been the focus of these experiments include plenum airflow pattern and velocity, plenum air temperature distribution, and total heat exchange between the exposed concrete structural slab, the underside of the raised floor, and the supply air as it flows through the underfloor plenum. Experimental data have been collected for comparison with and validation of the numerical calculations. A CFD model using a commercial software package has been developed to match the full-scale test facility and finely tuned to replicate the experimental measurements.

A review of the literature yields few references related to modeling of underfloor air supply plenums. Fujita and Tomiie (1999) developed a model to estimate the convective heat transfer coefficients between the plenum air and the concrete slab below and the underside of the raised floor panels above. However, this approach did not address the variation of the heat transfer coefficient at different locations of the plenum (due to differences in velocity) and how to extend the model to plenums with different design parameters, such as shape, size, and inlet velocities. Nagase et al. (1995) measured the cooling load of a UFAD test chamber and compared that with the return air extraction rate. Data showed that the cooling load was substantially greater than the return air extraction rate. The agreement was improved with insulated access floor, which indicated that the discrepancy might be due to the heat transfer from room into the underfloor supply plenum through the floor panel.

In this section we (1) describe the underfloor air supply plenum test facility and the accompanying data acquisition system, (2) describe the CFD plenum model, and (3) describe the validation of the CFD model by comparison with the experimental data.

## 2.2 EXPERIMENTAL FACILITY

### 2.2.1 UNDERFLOOR PLENUM.

The underfloor air supply plenum test facility was installed in December 2000 in a university warehouse building with an exposed concrete slab floor. Figure 1 shows plan and section views of the plenum structure. The plenum is 22 ft (6.7 m) by 74 ft (22.6 m) and 1 ft (0.305 m) high. The raised floor system was constructed from commercially available floor panels and included 16 variable-air-volume (VAV) floor diffusers. The plenum occupies three bays defined by 25 ft

(7.6 m) on center columns in the warehouse, with one edge bordering an exterior wall. A heating, ventilating, and air-conditioning (HVAC) system delivers supply air at a controlled temperature and volume into the underfloor plenum. The HVAC system has 2,330 cfm (1100 L/s) as the maximum supply airflow and 55-90°F (13-32°C) as the operable temperature control. The plenum inlet was installed at the middle of the side wall next to the HVAC system. In order to reduce the cost of instrumentation and CFD modeling, the plenum was afterwards divided into two parts by a plastic partition depicted in Figure 1 by a dashed line. Testing and modeling were accomplished on the left section of the plenum in Figure 1. The plenum section is 22 ft (6.7 m) by 48 ft (14.6 m), which is approximately two thirds of the original size. As shown in Figure 1, ten diffusers fall into this part of the plenum. The gaps between the floor panels and plenum edges were taped to eliminate air leakage for purposes of comparison with the CFD model predictions. The floor panels are 2 ft × 2 ft x 1.3 in. (0.6 m × 0.6 m x 0.033 m) constructed from a welded steel outer shell filled with a lightweight cementitious material. The thermal conductivity of a bare panel is 1.359 Btu-in/hr-ft<sup>2</sup>-°F (0.196 W/m-K) and that of a panel with carpet tiles is 1.002 Btu-in/hr-ft<sup>2</sup>-°F (0.144 W/m-K). These thermal properties were obtained from manufacturer's test data. The plenum is built on a structural concrete slab 10 in. (0.254 m) thick with thermal conductivity of 0.54 Btu/hr-ft-°F (0.93 W/m-K).

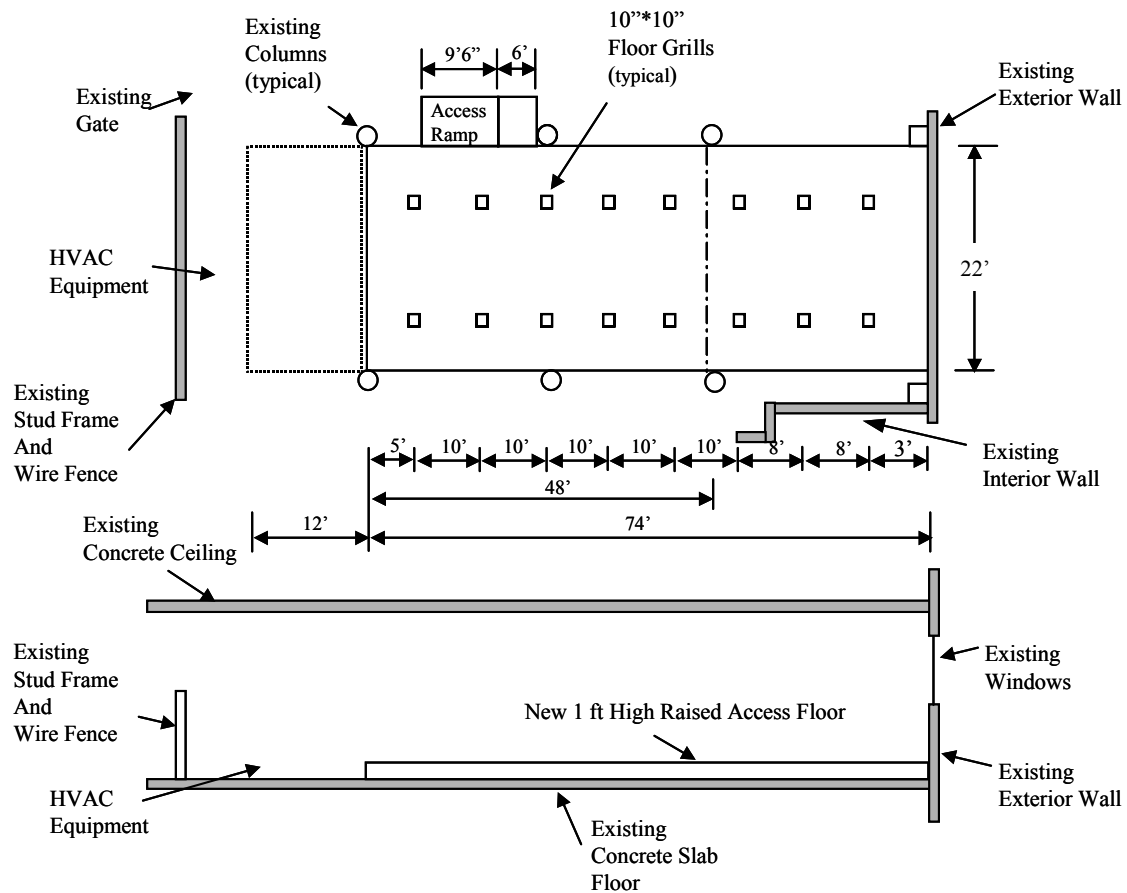


Figure 1. Plan and section views of underfloor air supply plenum test facility

### 2.2.2 PLENUM INLET CONFIGURATIONS

Preliminary calculations showed that the inlet configuration can have a significant impact on the plenum air temperature variation and heat gain. Two different inlet configurations were installed and tested to provide validation data for the CFD model. They are one single focused jet and two jets, which is a simplified version of an inlet vane configuration that produces multiple jets. Schematic diagrams of the single focused jet and inlet vanes/two jets inlet configurations are shown in Figure 2.

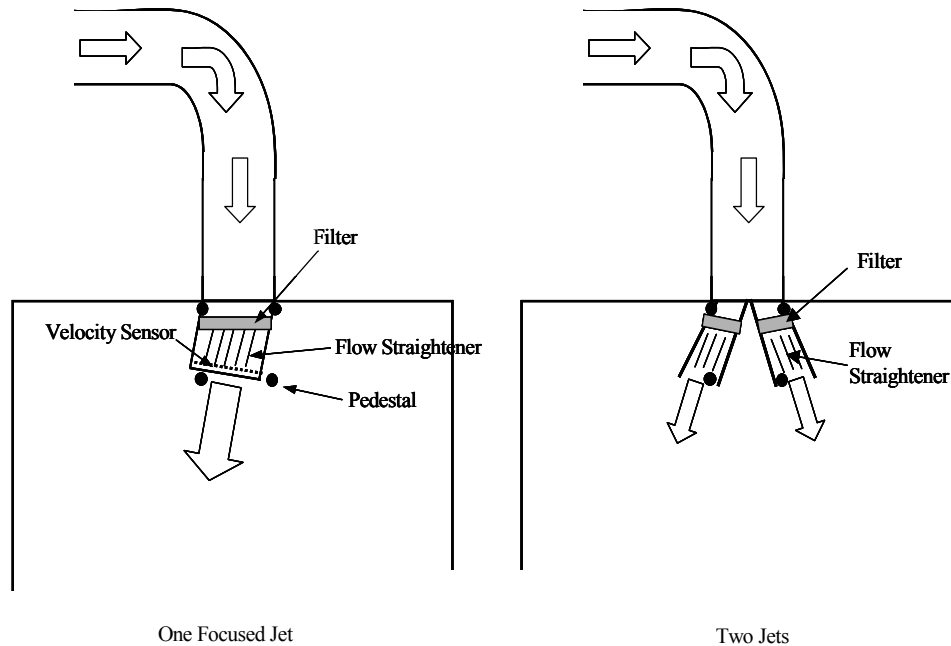


Figure 2. Schematic diagram of the single focused jet and inlet vanes/two jets inlet configurations

1. Single focused jet:

Flow straighteners and filter material are used to establish relatively uniform inlet airflow conditions, allowing more precise specification of the inlet conditions within the CFD model. It is noted that the direction of the single focused jet is not perpendicular to the short side of the plenum. The plenum inlet is located at the middle of the short side of the plenum. Thus, the geometry may be looked upon as simply symmetric. However, a symmetric geometry does not necessarily ensure a symmetric flow pattern. First, it is challenging to obtain a completely uniform inlet velocity throughout the cross-sectional area of the inlet. Secondly, due to the random and asymmetric nature of the turbulent flow, the airflow for the given single focused inlet jet configuration and plenum shape will not produce a perfectly symmetric pattern. In addition, information about an unrealistically symmetric flow pattern may not be normally useful in practice. In order to bypass the complexity introduced by the symmetric geometry, the direction of the inlet jet was turned to one side by a small angle.

2. Inlet vanes/Two jets:

Inlet vanes are one approach to spread out and slow down the inlet airflow. In this case, the inlet airflow can be represented experimentally as a collection of individual jets. Initial experiments and calculations indicated that the airflow pattern and air temperature distribution were very sensitive to the direction and momentum of each inlet jet. For the sake

of simplicity, two jets were fabricated to investigate the influence of the inlet-vanes configuration.

### 2.2.3 MEASUREMENT SET-UP

Type T thermocouples and a modular data acquisition and control system were installed to monitor air temperatures at the plenum inlet, floor diffusers, and selected locations inside the plenum. Four-inch (100-mm) deep holes were drilled at selected locations of the slab to obtain vertical slab temperature measurements at 1-in. (25-mm) intervals. Since there is no control on the heat transfer from under the slab (a loading dock is located on the floor below in the warehouse), the vertical temperature profile of the slab is very useful to implicitly derive the boundary conditions for the CFD simulation. Space air temperatures were measured just above the raised floor panels to obtain the boundary conditions above the plenum. If the heat transfer through the sidewalls of the plenum is neglected, the total heat gain into the plenum is the sum of heat transfer through the floor panels and concrete slab. In addition to convective heat transfer from the room air to the raised floor panels, recent research findings have shown that the radiative heat transfer from the warm ceiling (especially in a stratified UFAD space) to the floor could account for the majority of the heat gain through the floor panels into the plenum (Bauman et al. 2006). Therefore, the ceiling temperature needs to be considered as an important part of the specification of the boundary conditions above the plenum. It was measured using an infrared temperature sensor.

The plenum inlet air velocity is measured by a low air velocity and air temperature measuring system, with a cylindrical (directional) probe. The readings are then converted into the plenum inlet air supply volume by applying the cross-sectional area of the inlet opening. The air velocities at selected locations inside the plenum are measured by the same system, with a spherical (omni-directional) probe. The cylindrical and spherical probes provide the measurement range of 0.15 m/s (30 ft/min) to 10 m/s (2,000 ft/min) and 0.05 m/s (10 ft/min) to 5 m/s (1,000 ft/min), respectively. Both probes have the accuracy of  $\pm 3\%$  of the readings. The voltage outputs of the anemometers are connected to the existing data acquisition system.

For the slab and floor heat flux measurements, a heat flux transducer has been used. The thermal flux meter is a solid state, flat plate transducer designed to measure heat flux directly. The meter is placed upon any surface through which the heat flow is to be measured. The heat flux meter has an accuracy of 1% of the reading. Four flux meters were attached to the selected locations at the top surface of the slab and floor panel. The voltage outputs of the flux meters are also connected to the existing data acquisition system.

Figure 3 shows the locations selected to place the sensors for the air temperatures, velocities and slab/floor heat flux. Based on preliminary experimental observation and CFD simulation, the measurements at these key locations were used to characterize the predominant airflow pattern, air temperature distribution, and heat transfer from above and below the plenum. Experimental data collected under steady state conditions for the two different inlet configurations were used to validate the CFD plenum model described below.

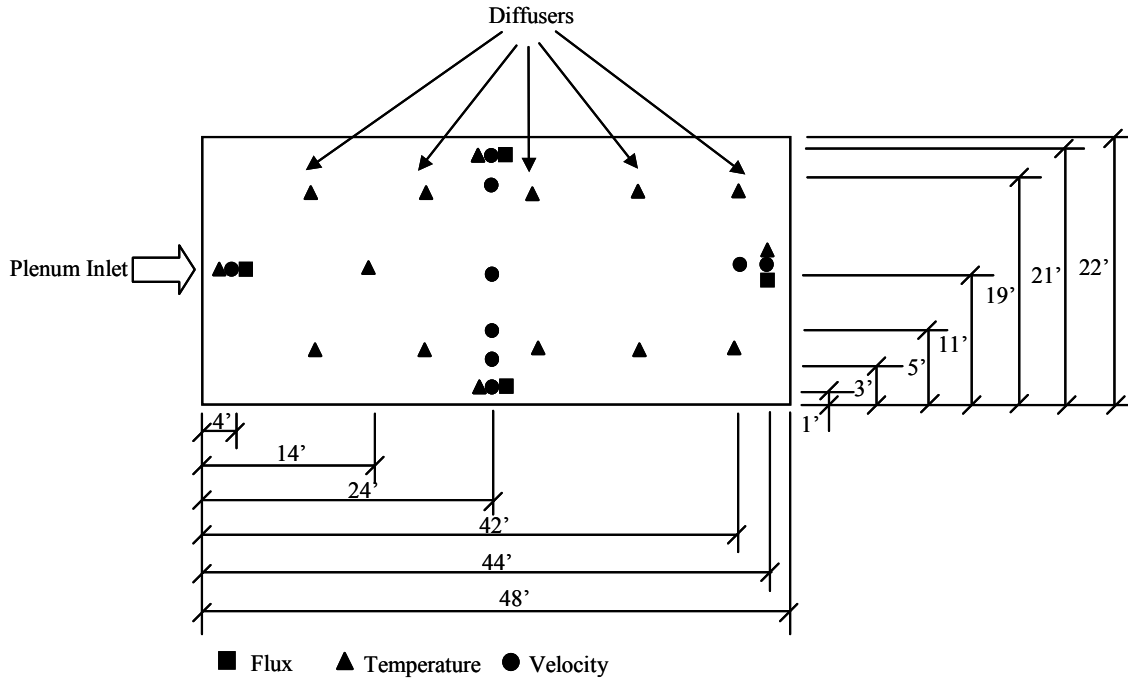


Figure 3. Locations of the sensors of the data acquisition system

## 2.3 DESCRIPTION OF THE CFD MODEL

The use of CFD modeling is increasing for solving flow and heat transfer problems within the heating, ventilating and air-conditioning (HVAC) industry. CFD programs provide a detailed analysis of the thermal fluid phenomena, producing simulation results that include qualitative values, such as airflow pattern, and quantitative values, such as air velocity, temperature, turbulence kinetic energy, Reynolds stress and surface heat flux. These parameters reported by the CFD code can be used in comparison with the experimental data. Generally speaking, air velocity and temperature can be simulated and measured with greater accuracy than the other parameters in both CFD and experimental applications. Since determining the overall heat gain into the plenum is one of the primary objectives of this ongoing research, heat flux was another important parameter involved in the comparison between the CFD simulation and experiment.

### 2.3.1 GOVERNING EQUATIONS

The partial differential equations solved by the CFD code are the unsteady Navier-Stokes equations in their conservation form. The instantaneous equations of mass, momentum and energy conservation can be written as follows.

**The continuity equation:**

$$\frac{\partial \rho}{\partial t} + \nabla \cdot (\rho \mathbf{U}) = 0 \quad (1)$$

where

$\rho$  = density, kg/m<sup>3</sup> or lb/ft<sup>3</sup>

$\mathbf{U}$  = velocity vector, m/s or ft/min

### **The momentum equation**

$$\frac{\partial \rho \mathbf{U}}{\partial t} + \nabla \cdot (\rho \mathbf{U} \times \mathbf{U}) = \nabla \cdot \left\{ -p \delta + \mu \left[ \nabla \mathbf{U} + (\nabla \mathbf{U})^T \right] \right\} + S_M \quad (2)$$

where

$\mu$  = dynamic viscosity, mPa-s or centipoise

$S_M$  = momentum source, kg/m<sup>2</sup>-s<sup>2</sup> or lb/ft<sup>2</sup>-min<sup>2</sup>

### **The energy equation**

When the contribution of the kinetic energy to the total energy can be neglected,

$$\frac{\partial \rho h}{\partial t} + \nabla \cdot (\rho \mathbf{U} h) = \nabla \cdot (\lambda \nabla T) + S_E \quad (3)$$

where

$h$  = specific static enthalpy, J/kg or ft-lb<sub>f</sub>/lb

$\lambda$  = thermal conductivity, W/m-K or Btu/h-ft-°F

$S_E$  = energy source, kg/m<sup>1</sup>-s<sup>3</sup> or lb/ft<sup>1</sup>-min<sup>3</sup>

## **2.3.2 CFD MODELS, AUXILIARY HEAT TRANSFER AND FLOW MODELS**

The turbulence model chosen for the simulation is a standard k-ε model (Launder and Spalding 1974). The k-ε turbulence model is a commonly used model and is suitable for a wide range of applications. As one of the most prominent turbulence models, it has been implemented in most general purpose CFD codes and is considered the industry standard model. Distinguished from the typical indoor airflow, which is a mixed convection, the flow in the plenum is generally forced convection flow due to the relatively high velocity and the existence of pedestals as the cause of turbulence throughout the entire domain. The comparison between the experimental data and model predictions discussed in the following sections shows that the k-ε model can be used with acceptable accuracy.

Depending on the simulation, five heat transfer model options are possible. They are none, isothermal, thermal energy, total energy and fluid dependent. The heat transfer model selected for the simulation is the thermal energy model. The thermal energy model neglects high speed energy effects and is therefore suitable for low speed flow applications. The heat transfer model is used to predict the plenum heat gain and air temperature variation in the plenum.

### **2.3.2.1 Boundary conditions**

The dimensions of the plenum inlet were 10.7 in. × 24 in. (0.272 m × 0.6096 m) and the measured inlet air velocity was 900 fpm (4.5 m/s) for both experiments. The plenum outlet boundary condition is set to zero relative static pressure. Since the plenum is only 1 ft (0.305 m) high, the area of the plenum sidewalls compared with those of the floor and slab is relatively small. Hence, heat transfer through the sidewalls is neglected and the thermal boundary condition at the sidewalls is set to be adiabatic. The heat gain is therefore assumed to be only from the top and bottom surfaces of the plenum. It is noted that previous research has shown that the radiation from the ceiling of a stratified UFAD space is the dominant driver for the rate of heat transfer through the top surface (raised floor panels) of the plenum (Bauman et al. 2006).

More details about the boundary conditions used for the CFD simulations are depicted in Figure 4. The boundary conditions above the plenum include ceiling temperature  $T_{ceiling}$ , ceiling emissivity  $e$ , and view factor from ceiling to the top surface of the raised floor  $F$ . The view factor is assumed to be 1.0 since there were no obstructions (e.g., furniture) in the warehouse to block the thermal radiation from the ceiling to the floor. The boundary conditions under the plenum include air temperature  $T_{air}$  and convection coefficient  $h_c$ . The boundary conditions at the plenum inlet include the inlet temperature  $T_{in}$ , airflow volume  $V$ , and inlet velocity  $v$ .

It should be clarified that this experiment was not an effort to duplicate any practical operating conditions in a real UFAD system. The plenum was installed in a warehouse where there was no control of the thermal conditions above and below the plenum. Hence, a relatively low plenum supply air temperature was maintained to establish a substantial temperature difference between the plenum and its surroundings.

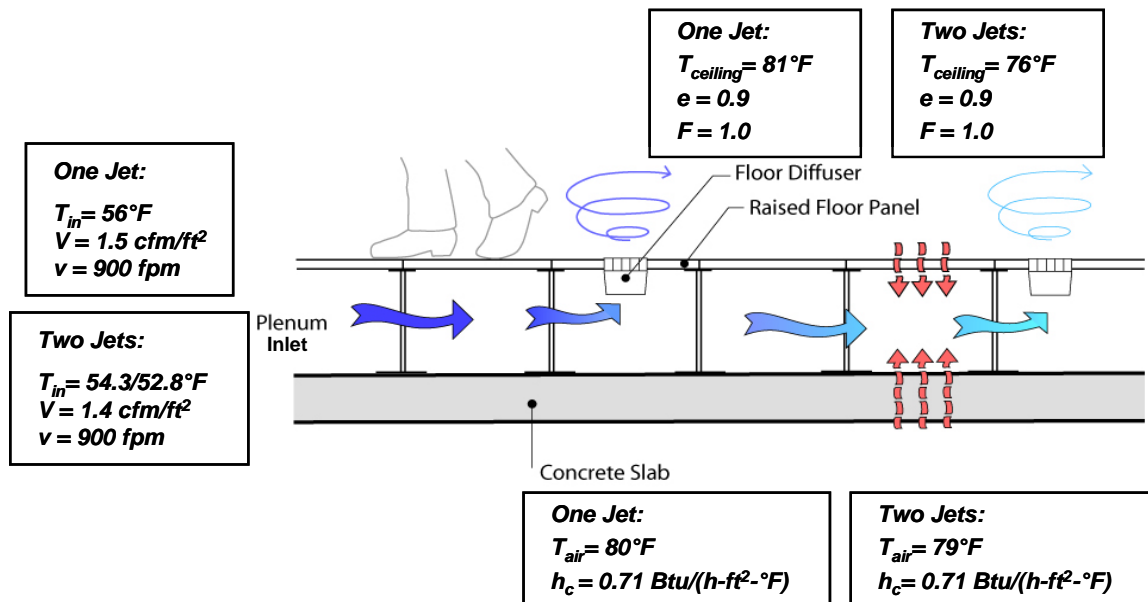


Figure 4. Boundary conditions of the CFD simulation for the single focused jet and inlet vanes/two jets inlet configurations (IP Units)

### 2.3.2.2 Source term: Resistance of pedestals

Preliminary comparisons showed that measured velocities were substantially lower than the CFD predictions when the resistance of the pedestals was neglected. There were two approaches available to represent the resistance of the pedestals in the CFD model.

1. Actually building the pedestals into the geometry of the CFD model. This approach generally ends up with a huge mesh size due to the resolution required between the pedestals. Hence, it requires a much more powerful computer than what is commonly available. Computation time may also be extended. In addition, building the geometry can be very labor intensive.
2. Adding a resistance to the fluid domain as a source term in the governing equation, to represent the resistance caused by the pedestals. Since the pedestals are uniformly distributed throughout the plenum, this approach is chosen for the CFD model due to its simplicity, efficiency and low requirement on the hardware (i.e., memory and CPU speed).

In the CFD plenum model, the resistance of the pedestals is represented by linear and quadratic resistance coefficients,  $C_{R1}$  and  $C_{R2}$ . An isotropic momentum source may be formulated using the generalized form of Darcy's law,

$$S_M = -C_{R1}U_i - C_{R2}|U|U_i \quad (4)$$

Where  $S_M$  is the momentum source term,  $\text{kg/m}^2\text{-s}^2$  or  $\text{lb/ft}^2\text{-min}^{-2}$ ,  $U_i$  is the velocity,  $\text{m/s}$  or  $\text{ft/min}$ . The momentum source term  $S_M$  is incorporated into Equation 2 to solve the affect of the resistance of the pedestals on the airflow velocity in the plenum.

### 2.3.2.3 Numerical methods

Parameters for the grid size and quality, such as global element scale factor and global element seed size, were set. The rest of the discretization process is accomplished automatically by the CFD code. The auto time step was selected. This option uses an internally calculated physical time step size based on the specified boundary conditions, initial guesses, and geometry of the domain. It does not require prior knowledge of the approximate time step size for the particular problem. The numerical scheme was set to high resolution. With this setting, the blend factor values vary throughout the domain based on the local solution field. In flow regions with slow changing gradients, the blend factor will be close to 1.0 for accuracy. In areas where the gradients change sharply, the blend factor will be closer to 0.0 to prevent over- and under-estimates and to maintain robustness.

## 2.4 COMPARISON OF MODEL PREDICTIONS WITH EXPERIMENTAL DATA

The comparison has been based on a steady state simulation. Since the test facility does not have control of the thermal conditions surrounding the plenum (e.g., space above and floor below the plenum), it is impractical to obtain the experimental data under complete steady state conditions. However, due to the fact that the thermal conditions in the large warehouse building containing the test facility and its accompanying systems usually are quite stable and do not experience rapid changes, data collected from quasi steady state conditions are acceptable for use in the comparison with theoretical calculations. In the experiment, we delivered a constant temperature and volume of air for at least 72 hours before taking measurements. All of the transient behaviors were minimized after such a relatively long time. Data showed that the variation of temperature and heat flux was negligible during the short period of time (typically 15 minutes) used for the data collection period.

Generally, the comparison of CFD results with the experimental data is the most important part of the reporting process for an indoor environment CFD analysis. The quantitative comparison between CFD predictions and experimental data includes temperature at each diffuser, plus air velocity and slab heat flux at selected locations in the plenum. These data were directly measured in the experiment. The plenum heat gain was calculated based on the measured inlet/outlet temperature difference (where the outlet temperature represents the average of all measured diffuser temperatures) in combination with the airflow volume in the experiment. It can also be computed from CFD results using the same approach. In addition, the heat transfer into the plenum from above the floor and under the slab is obtained from the CFD results. It can be compared against the heat gain of the plenum using temperature and air volume approach in order to check the convergence of the CFD calculations.

### 2.4.1 AIRFLOW PATTERN

The first step is as simple as a smoke visualization that gives a qualitative comparison for the airflow pattern in the plenum. Figure 5 shows the streamline plots for the single focused jet inlet configuration. The airflow pattern for this case was also investigated using smoke visualization in the test facility. In Figure 5, a big recirculation originating at the plenum inlet and defined by the dimensions of the plenum is observed. The CFD computed flow pattern agrees very well with that by the smoke visualization. It is noted that the non-uniformity of the air temperatures at diffusers

can be clearly explained by this circulation flow pattern. For the two jets inlet configuration, the big circulation is broken into two relatively small circulations. The shape of the plenum and locations of the inlet and diffusers allow each of the two jets to serve half of the plenum area and diffusers separately in this case. The two jets enter into the plenum from one of the short sides, turn toward the long sides and flow along these long edges separately until reaching the opposing short side of the plenum. When the two jets reach the far end, they turn around, meeting with each other near the midpoint of the far side, and flow back toward the plenum inlet through the central region of the plenum, creating two similar sized recirculation patterns having the full length of the plenum but only half the width.

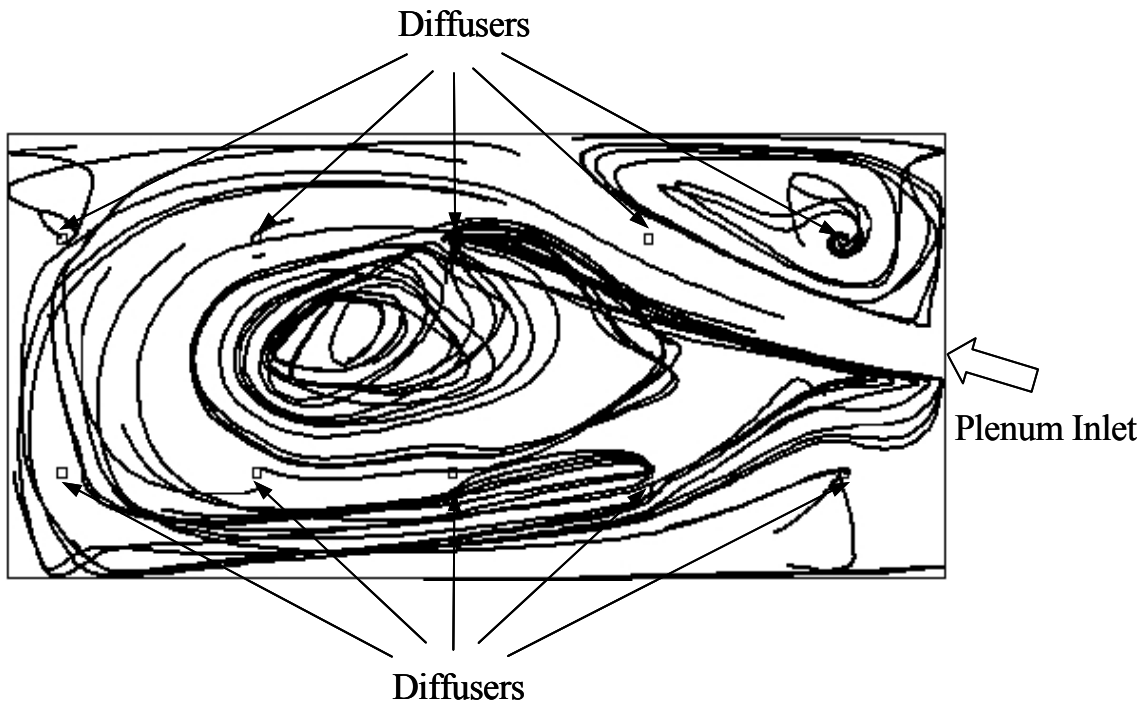


Figure 5. CFD simulated airflow pattern of the single focused jet inlet configuration

#### 2.4.2 AIR VELOCITY

Figures 6 and 7 present contour plots of the predicted velocity distributions at mid-height of the plenum for the focused jet and two jets inlet configurations, respectively. Each number in the contour plot represents the average air velocity over the indicated area. In addition, the measured and computed air velocities at selected measurement locations in the plenum are shown. The measured velocities agree quite well with the experimental data. The velocity plot also agrees well with the airflow pattern observed through the use of smoke visualization. Due to the resistance offered by the pedestals, the air velocity decreases so fast that the magnitude of the velocity over most of the area of the plenum is lower than 180 ft/min (0.91 m/s). Hence, it may be reasonable to assume that the overall convective heat transfer coefficient inside the plenum is fairly close to that of natural convection.

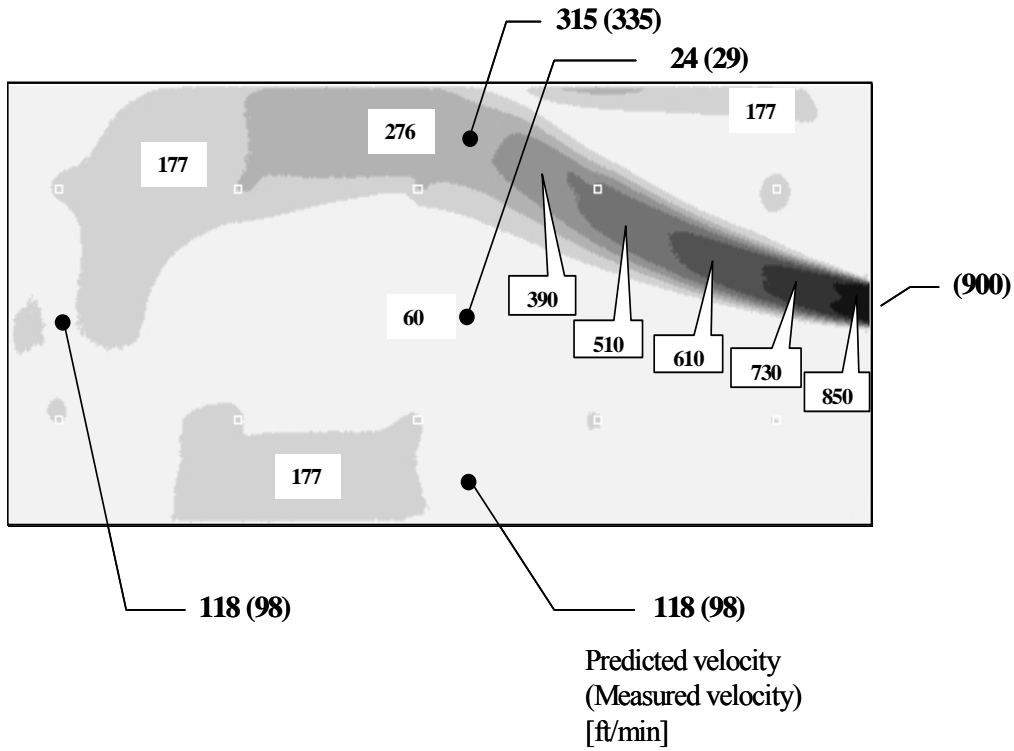


Figure 6. Comparison of measured and CFD predicted plenum air velocity for single focused jet inlet configuration (IP Units)

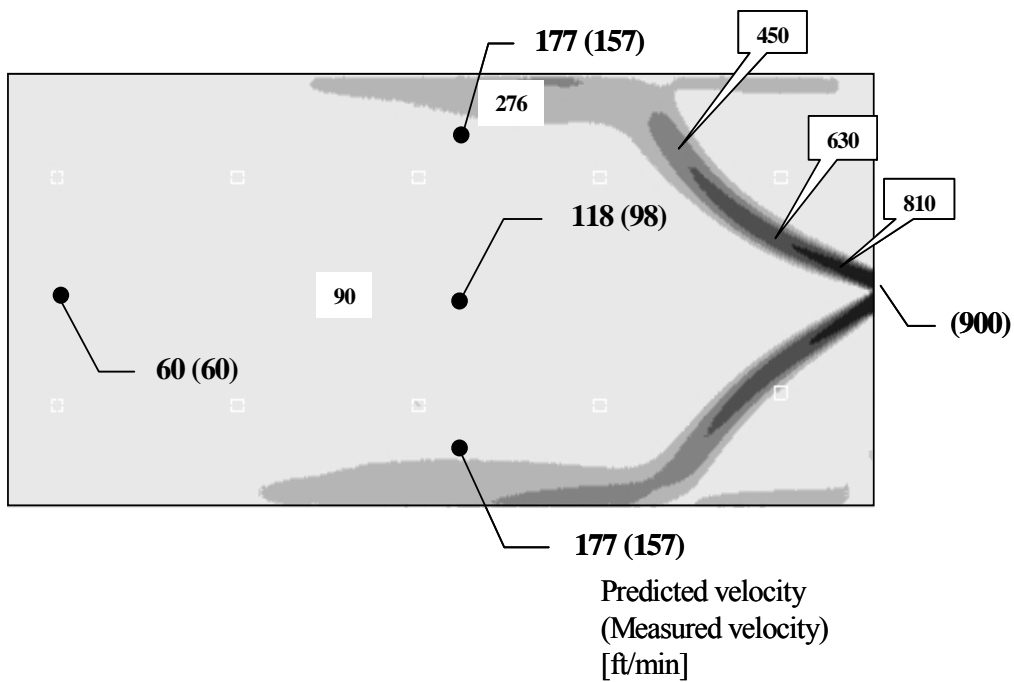


Figure 7. Comparison of measured and CFD predicted plenum air velocity for inlet vanes/2 jets inlet configuration (IP Units)

### 2.4.3 TEMPERATURES AT DIFFUSERS

Figure 8 presents a contour plot of the predicted temperature distribution at mid-height of the plenum for the focused jet inlet configuration. Each number in the contour plot represents the average air temperature over the indicated area. In addition, the measured and computed temperatures at each of the ten diffusers are shown. Figure 9 presents the comparison of the measured and predicted diffuser temperatures in numerical order for this same inlet configuration. For the focused jet case, the difference between the highest and lowest diffuser temperatures is approximately 10°F (5.6°C). It is observed that diffuser #2, located within the inlet jet depicted in Figure 8 by the lightest color, has the lowest temperature, and one of the diffusers located closest to the plenum inlet (#6) has the highest. The flow pattern shown in Figure 5 helps to explain this result. The overall plenum temperature plot in Figure 8 is consistent with the flow pattern. The diffuser that has the lowest temperature is the first one directly impacted by the inlet jet. The diffuser that has the highest temperature is the last one impacted by the expanded airflow pattern, having traveled to the far end of the plenum before recirculating back to the nearby diffuser. This analysis helps to explain observations made in many underfloor supply plenum applications. The diffusers closest to the plenum inlet do not necessarily have the lowest temperatures. The temperature rise depends upon the distance that the inlet air travels before reaching the particular diffuser. Due to the complexity of the airflow pattern for a given plenum shape and inlet configuration, the traveled distance is not necessarily the same as the geometric distance between the inlet and diffuser under many conditions.

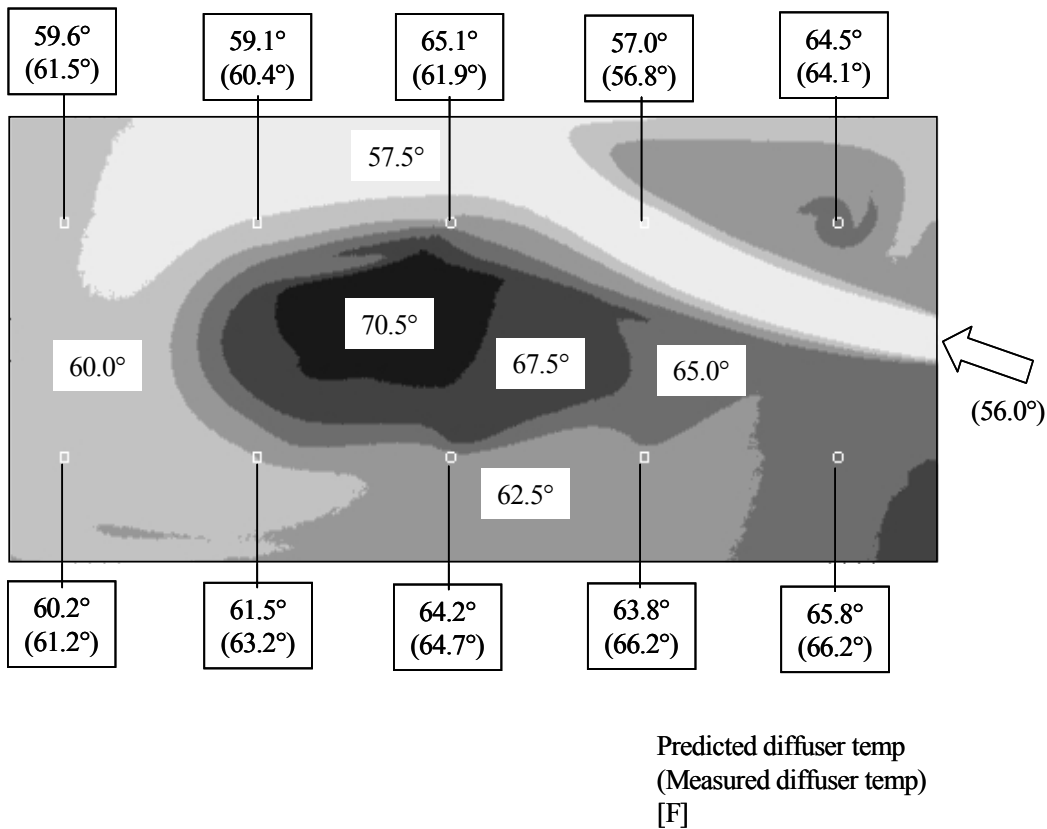


Figure 8. Comparison of measured and CFD predicted diffuser temperatures for single focused jet inlet configuration (IP Units)

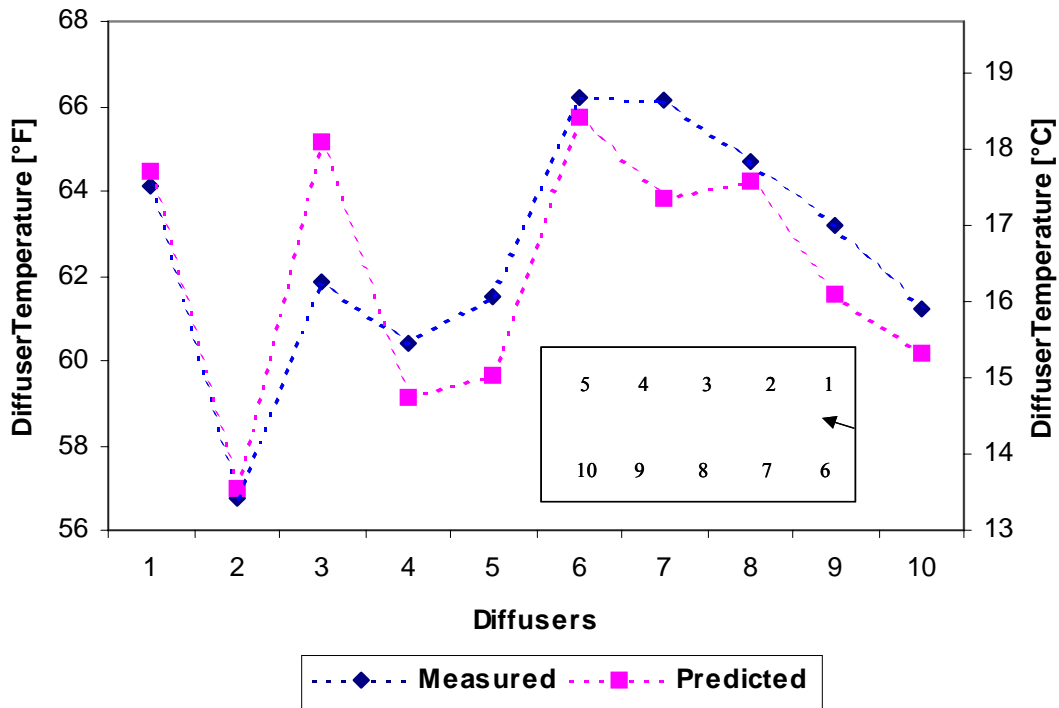


Figure 9. Comparison of measured and CFD predicted diffuser temperatures for single focused jet inlet configuration

Figure 10 presents a contour plot of the predicted temperature distribution at mid-height of the plenum for the two jet inlet configuration. Each number in the contour plot represents the average air temperature over the indicated area. In addition, the measured and computed temperatures at each of the ten diffusers are shown. Figure 11 presents the comparison of the measured and predicted diffuser temperatures in numerical order for this same inlet configuration. For the two jets inlet configuration, the difference between the highest and lowest temperatures is less than 5°F (2.8°C). As discussed earlier, the flow pattern in this case allows the average distance that the air travels before leaving each diffuser to be shorter than the single jet case. As a result, the non-uniformity of the diffuser air temperatures is greatly improved for this flow pattern.

Table 1 presents the comparison of the non-uniformity of the diffuser temperatures between the single focused jet and two jets inlet configurations. In particular, the standard deviation calculation indicates that the two jets inlet configuration provides more evenly distributed diffuser temperatures throughout the entire plenum.

Table 1. Comparison of the temperature rise and standard deviation for different inlet configurations

	One Jet	Two Jets
Supply Temperature °C (°F)	13.3 (56.0)	12.0(53.6)
Average Diffuser Temperature °C (°F)	17.0 (62.6)	15.1 (59.2)
Standard Deviation for the Diffuser Temperatures °C (°F)	1.6 (2.9)	0.8 (1.4)

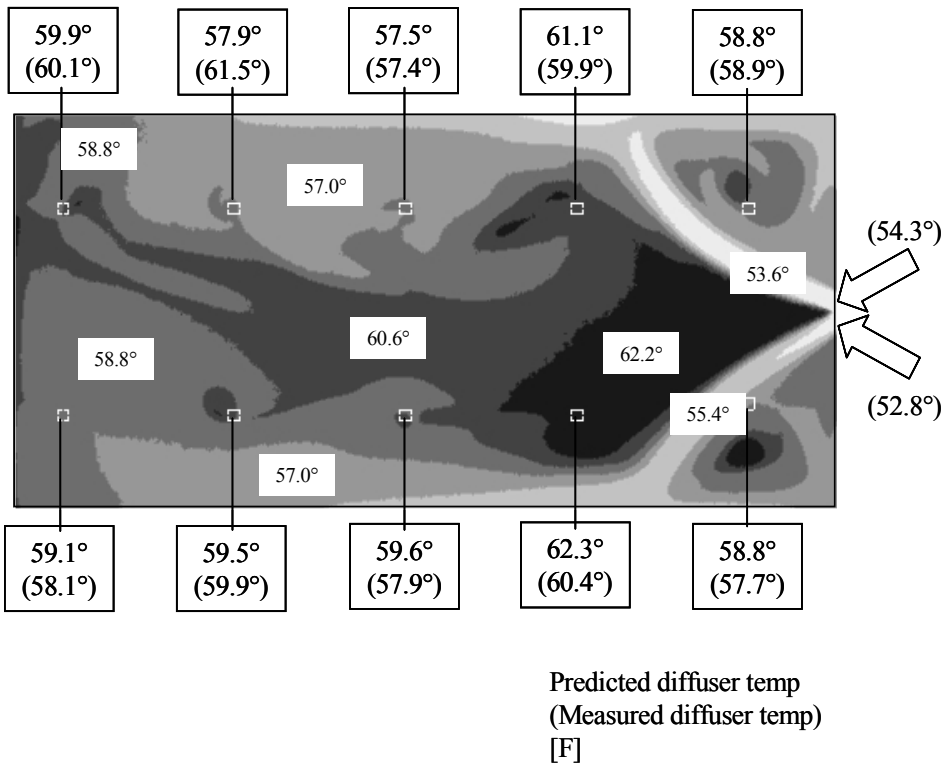


Figure 10. Comparison of measured and CFD predicted diffuser temperatures for inlet vanes/two jets inlet configuration (IP Units)

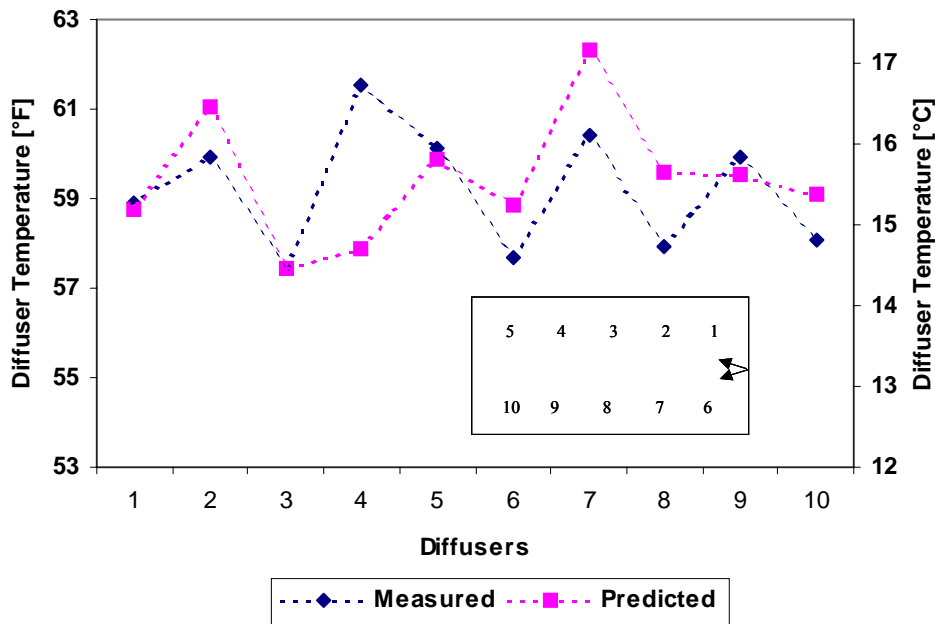


Figure 11. Comparison of measured and CFD predicted diffuser temperatures for the two jets inlet configuration

#### 2.4.4 SLAB HEAT FLUX

The experiments also measured the slab surface heat flux at selected locations. Results indicate that the heat flux has its highest magnitude at locations closest to the inlet, where the highest velocities are observed. When the airflow travels farther into the plenum and slows down, the heat flux decreases accordingly. It is commonly recognized that the convective heat transfer coefficient decreases as velocity decreases. Meanwhile, the temperature difference between the air in the plenum and its boundaries becomes smaller as the plenum air temperature rises.

Therefore, among the four selected measurement locations shown in Figure 3, the highest heat flux takes place at the plenum inlet and the smallest heat flux is observed at the location where the velocity is the lowest and distance the airflow has traveled is the longest. Table 2 shows the comparison of the total heat gain of the plenum between experiment and CFD prediction.

Although the test facility does not allow the split of total heat gain into heat transfer through the floor and concrete slab, the CFD model is capable of providing this relatively detailed information. Agreement for the total heat gain into the plenum is found to be within 7% for the single focused jet and within 5% for the two jets inlet configuration.

Table 2. Comparison of heat gain into the plenum between test and CFD prediction

	One Jet		Two Jets	
	Measured W (Btu/h)	Predicted W (Btu/h)	Measured W (Btu/h)	Predicted W (Btu/h)
Floor	N/A	1,322 (4510)	N/A	1,612 (5,500)
Slab	N/A	1,753 (5981)	N/A	1,379 (4,705)
Total	3,305 (11,276)	3,075 (10,491)	2,851 (9,727)	2,991 (10,205)

## 2.5 DISCUSSION OF RESULTS

While experimental testing has been conducted successfully using a full-scale test facility, the CFD modeling and simulation of the underfloor supply plenum represents a relatively speedy and economical alternative to experimental studies. The CFD analysis can incorporate the actual details of the geometry, material properties, and boundary conditions to produce complete and detailed information about the distribution of temperature, velocities, etc. In order to validate the CFD model, the experimental testing is necessary. On the other hand, the CFD prediction has been used to plan and design the experiment, to significantly reduce the amount of experimentation, and to supplement and enrich the experimental results.

CFD predictions show that the directions of airflow at the inlet of the plenum play an important role in the formation of the flow pattern. As a result of different airflow patterns, the temperature distribution, heat flux distribution and total heat transfer may vary significantly. In order to carefully validate the CFD model, experiments were conducted for two different plenum inlet configurations: one single focused jet and two separated jets. The boundary and test conditions for these two experiments were replicated in the CFD model simulation. The CFD model was refined progressively based on the comparison with the full-scale testing data. The comparison between the final results of the model calculation and test data demonstrates that the CFD model is capable of simulating the plenum airflow pattern, temperature, velocity, heat flux and total heat transfer with acceptable accuracy.

For the given plenum shape, the major findings are as follows:

- The re-circulation is larger in size with one inlet jet than that with two jets.
- The temperature non-uniformity is greater with one inlet jet than that with two jets.
- Air velocity in the plenum is generally low for both inlet configurations, compared with the inlet velocity. The resistance of the pedestals may not be ignored.
- The magnitude of the heat flux from the slab into the plenum is associated with the air velocity and air temperature, since convective heat transfer is a product of convective coefficient and temperature difference. Airflow has its highest velocity and lowest temperature at the plenum inlet. Obviously, the heat flux decreases gradually after the airflow enters the plenum.

## 2.6 CONCLUSIONS

A CFD model for the underfloor supply plenum of an underfloor air distribution (UFAD) system has been developed. The model can be used to predict the airflow patterns, air temperature and velocity distributions, and heat flux from the structural slab and the raised floor into the plenum for a variety of thermal and airflow boundary conditions. The model has been validated using experimental data collected in a full-scale plenum test facility. The computed air temperature, velocity and heat flux generally agree well with the measured data. More importantly, the discrepancies between computed and measured total heat gain of the plenum are less than 10%.

The CFD plenum model developed here is readily extendable to other plenum configurations. In the following section, we will discuss the results from a series of sensitivity simulations using the validated CFD model to investigate a wider range of realistic underfloor air supply plenum configurations to extend the testing database from the limited number of full-scale test conditions. This expanded database has been used to develop the simplified plenum model for implementation in EnergyPlus.

### 3 DEVELOPMENT OF UNDERFLOOR PLENUM MODEL FOR ENERGYPLUS

---

In this section we describe the development of a simplified underfloor plenum model suitable for implementation into EnergyPlus. To accomplish this, we used the validated CFD plenum model (described in Section A.3.2) to conduct a larger number of “numerical experiments” to investigate the energy performance of underfloor plenums over a wide range of realistic plenum configurations and operating conditions. The goal of these CFD simulations was to generate a numerical database upon which a simplified plenum model could be constructed and tested by comparison. In the following sections, we report on the CFD sensitivity simulations and the formulation and final description of the simplified underfloor plenum heat balance model.

#### 3.1 CFD SENSITIVITY STUDY

##### 3.1.1 MODEL CONFIGURATIONS

The validated CFD model was used to simulate nine different plenum configurations to investigate the impact of inlet locations, inlet velocity, total airflow rate, inlet jet direction and plenum shape on the plenum heat gain and temperature distribution. Schematic diagrams of these different plenum configurations are shown in Figures 12-20. For most of the cases (Figures 12-18), the modeled plenum had the dimensions of 100 ft by 200 ft by 1 ft (0.3 m) high, representing a 20,000 ft<sup>2</sup> (1,860 m<sup>2</sup>) floor plate of a building. For these simulations, there were 60 diffusers in total, 28 in the perimeter zone and 32 in the interior zone. Figure 21 shows a schematic diagram of the boundary conditions established for most of the sensitivity analysis cases, except where noted below. These primary boundary conditions were as follows: inlet air temperature 62°F (16.7°C), airflow rate = 1 cfm/ft<sup>2</sup> (0.00508 m<sup>3</sup>/s-m<sup>2</sup>) or 20,000 cfm (9.44 m<sup>3</sup>/s) total, ceiling temperature = 78°F (25.6°C), ceiling emissivity = 0.9, view factor = 0.5, and temperature under slab = 80°F (26.7°C).

Figures 12-14 show the different cases studied for external inlet locations. Although not common in practice, this series of simulations investigated thermal performance in a large open plenum when plenum inlets were located around the perimeter of the building floor plate. Since direct shooting of the air into the interior zone would not be a good design practice (the coolest supply air is needed in the perimeter zones), the analysis was based on how to turn the inlet jets towards the perimeter zone instead. The airflow was divided into four jets at each of the four inlet locations (one along each side). The direction of each jet was defined by the angles  $\alpha$  and  $\beta$  shown in Figure 12. The two different combinations of angles investigated included the following: small angle ( $\alpha = 30^\circ$ ,  $\beta = 0^\circ$ ) and large angle ( $\alpha = 30^\circ$ ,  $\beta = 30^\circ$ ). Most cases used an inlet velocity of either 600 fpm or 1,200 fpm (Figure 12). Figure 13 shows a case with lower inlet velocities created by supplying air evenly along the two small perimeter edges of the plenum zone. For the theoretically lowest inlet velocity case, it was assumed that air is supplied evenly along all perimeter edges of the simulated plenum, producing an extremely low plenum inlet velocity (Figure 14). Most of the simulations used a total airflow rate of 1 cfm/ft<sup>2</sup> (5.08 L/s-m<sup>2</sup>). In addition, for the small angle configuration, simulations were made to investigate sensitivity to total airflow rate (0.5 cfm/ft<sup>2</sup>, 1.5 cfm/ft<sup>2</sup>, and 2.0 cfm/ft<sup>2</sup>) at a fixed inlet velocity or 1,200 fpm.

Figures 15-18 show the different cases studied for internal inlet locations. As indicated, air is delivered into the plenum from each end of a simulated core region of the floor plate in Figure 15, and from the same locations, but without the central core obstructions in Figure 16. In Figure 17, a case is investigated where all of the air is delivered to the plenum from only one of the two internal supply locations. Inlet velocities were assumed to be either 600 fpm or 1,200 fpm, except in the low velocity case of Figure 18. For that theoretically lowest inlet velocity case, it is assumed that air is supplied evenly along all edges of the simulated core region. Although it does

not represent a realistic design, this case may be looked upon as a baseline where the minimum heat gain (lowest average velocities) could be achieved.

For the case shown in Figure 15, simulations were made to investigate sensitivity to total airflow rate ( $0.5 \text{ cfm/ft}^2$ ,  $1.5 \text{ cfm/ft}^2$ , and  $2.0 \text{ cfm/ft}^2$ ) at a fixed inlet velocity or 1,200 fpm (Cases 4a, 4e, and 4f). Two additional simulations were made to investigate variations in the plenum inlet air temperature. These represent Cases 4g and 4h with plenum inlet temperatures of  $67^\circ\text{F}$  and  $57^\circ\text{F}$ , respectively. Simulations were also made to investigate variations in the assumed ceiling temperature, which radiates to the top surface of the raised floor. Cases 4i and 4j represent ceiling temperatures of  $73^\circ\text{F}$  ( $5^\circ\text{F}$  less than the baseline boundary condition of  $78^\circ\text{F}$ ) and  $83^\circ\text{F}$  ( $5^\circ\text{F}$  more than the baseline boundary condition of  $78^\circ\text{F}$ ), respectively. Finally, two simulations were made to investigate variations in the assumed return air temperature on the floor below, which drives the conduction up through the slab into the underfloor plenum. Cases 4k and 4l represent return air temperatures of  $75^\circ\text{F}$  ( $5^\circ\text{F}$  less than the baseline boundary condition of  $80^\circ\text{F}$ ) and  $85^\circ\text{F}$  ( $5^\circ\text{F}$  more than the baseline boundary condition of  $80^\circ\text{F}$ ), respectively.

Figures 19 and 20 show two special geometry plenum configurations. Figure 19 is a 100 ft by 100 ft square plenum with external inlet locations. Figure 20 is an L-shaped floor plate, also with external inlet locations. For both of the special geometries, the total airflow rate was held constant at  $1 \text{ cfm/ft}^2$  ( $5.08 \text{ L/s-m}^2$ ) and two different inlet velocities were simulated: 600 fpm and 1,200 fpm.

### 3.1.2 EXTERNAL INLETS

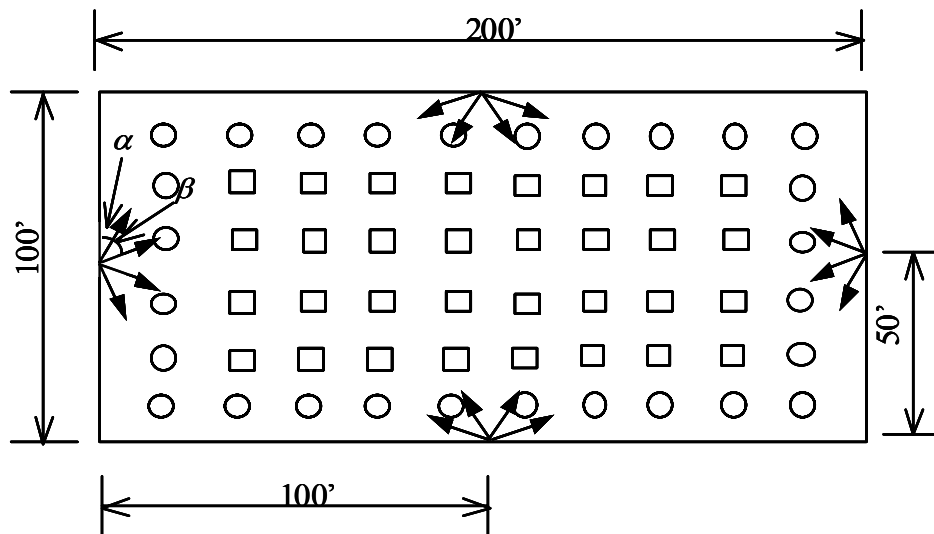


Figure 12. External inlets – Cases 1 a/b/c/d/e/f/g (varying the inlet velocity, airflow rate and inlet jet directions, i.e.,  $\alpha, \beta$  in the diagram)

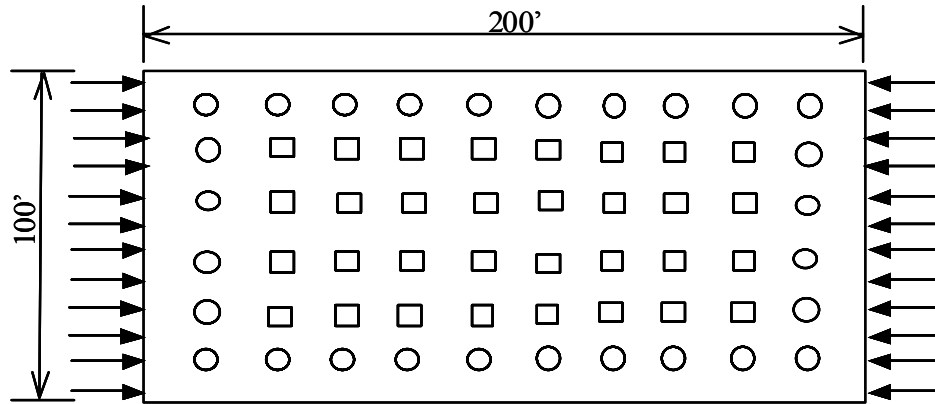


Figure 13. External inlets – Case 2, lower velocities

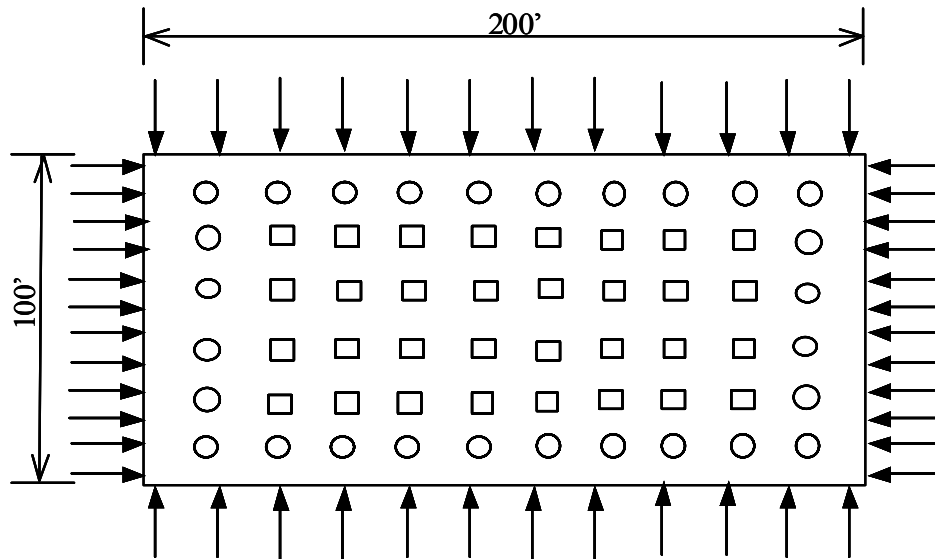


Figure 14. External inlets – Case 3, lowest velocities

### 3.1.3 INTERNAL INLETS

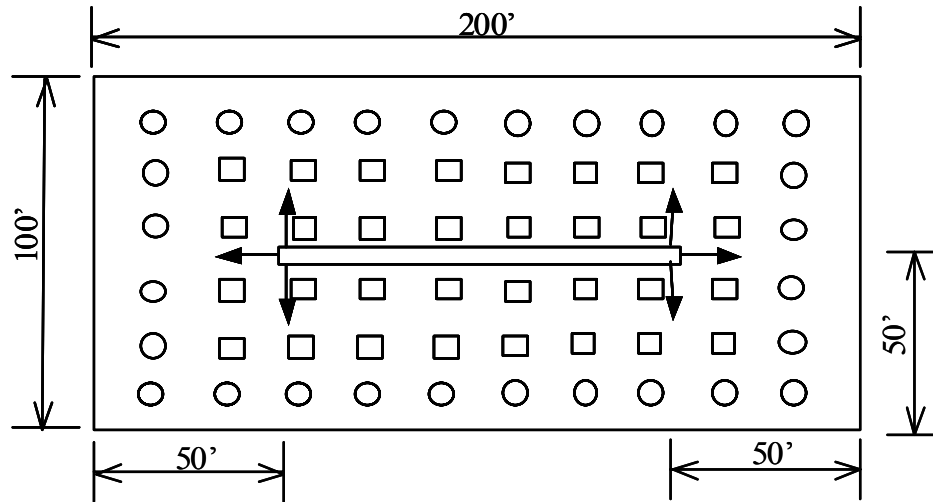


Figure 15. Internal inlets – Cases 4 a-l (varying the inlet velocity, airflow rate, plenum inlet temperature, ceiling temperature, and return air temperature on the floor below)

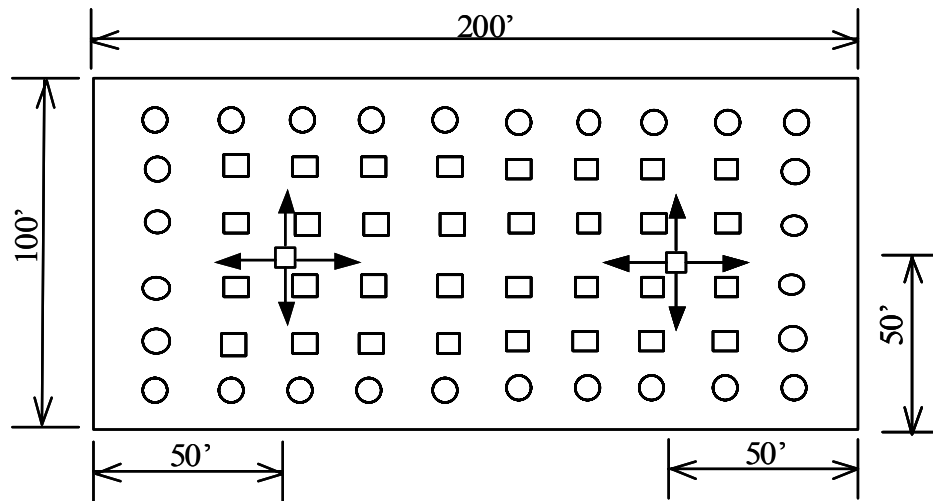


Figure 16. Internal inlets – Case 5

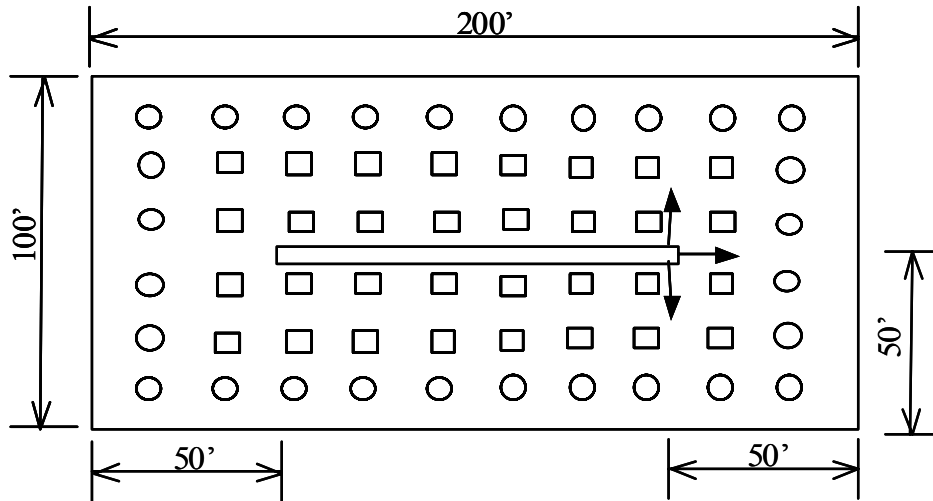


Figure 17. Internal inlets – Case 6

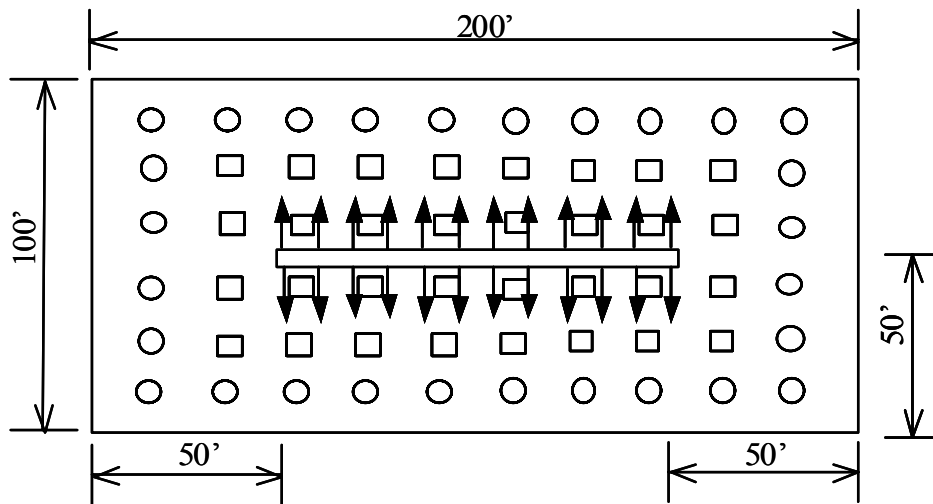


Figure 18. Internal inlets – Case 7, low velocity

### 3.1.4 SPECIAL SHAPES

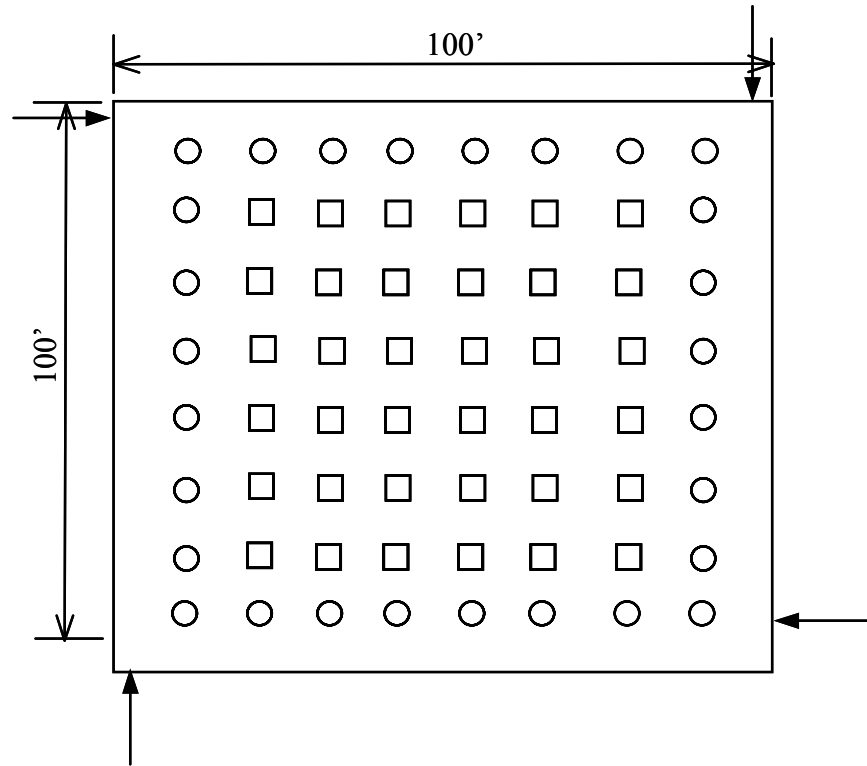


Figure 19. Special shapes – Case 8 a/b (varying the inlet velocity)

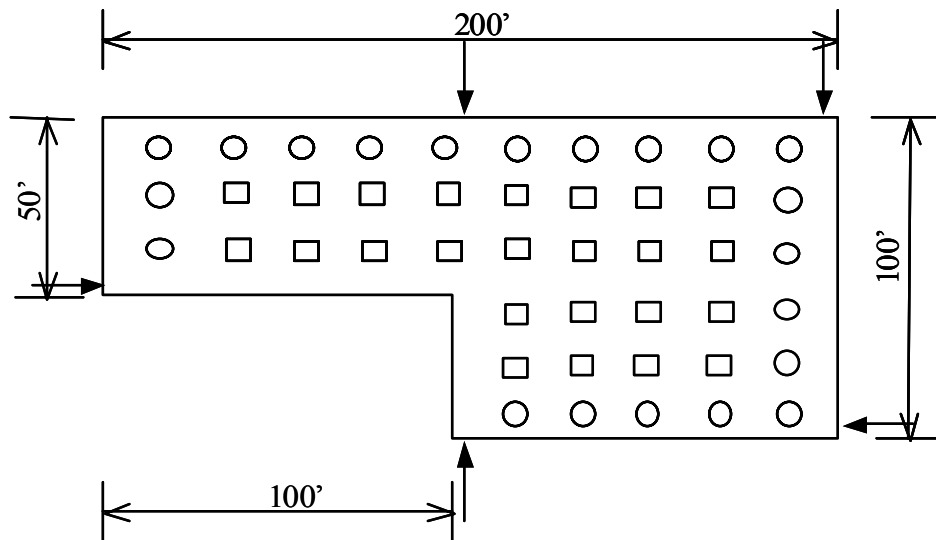
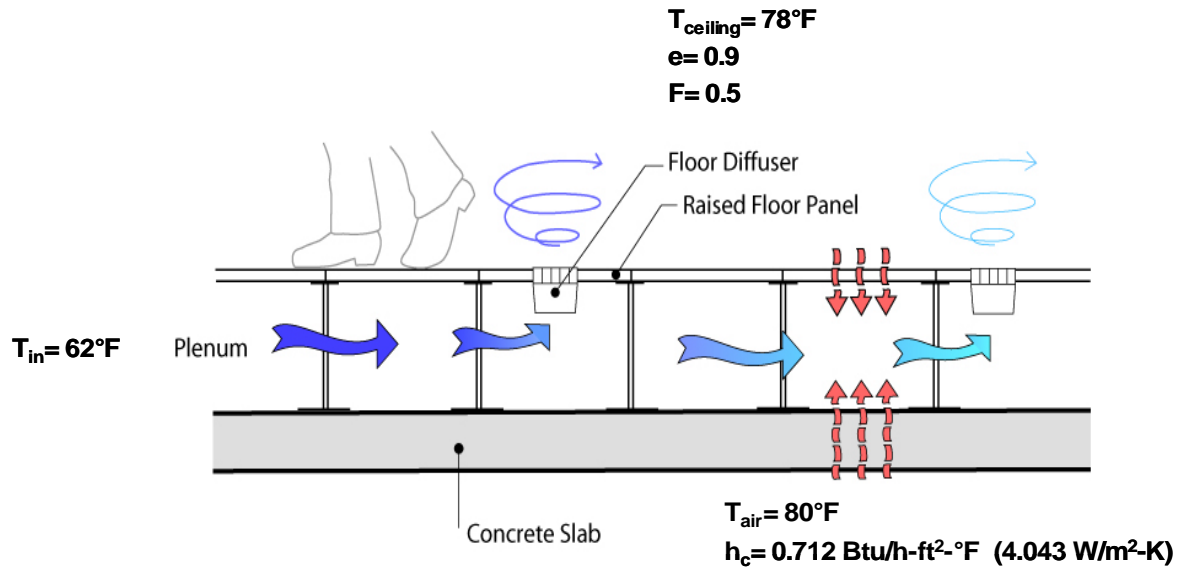


Figure 20. Special shapes – Case 9 a/b (varying the inlet velocity)



Floor conductivity = 1.36 Btu-in/h-ft<sup>2</sup>-°F ( 0.196 W/m-K)  
 Floor thickness = 1.3 inch  
 Slab conductivity = 6.46 Btu-in/h-ft<sup>2</sup>-°F ( 0.93 W/m-K)  
 Slab thickness = 6 inch

Figure 21. Boundary conditions for CFD plenum model sensitivity simulations

### 3.2 RESULTS

Table 1 summarizes the results for all cases simulated with the validated CFD plenum model. Table 1a presents results for external inlets (Cases 1-3), Table 1b presents results for internal inlets (Case 4), and Table 1c presents results for additional internal inlet configurations and special shapes (Cases 5-9). The predicted heat transfer variables include the total heat gain to the plenum (through both the concrete slab and raised floor panels), and the average surface convection coefficients for each of these two primary surfaces. Each convection coefficient is derived to predict the average heat flux based on the thickness and conductivity of each horizontal layer (floor or slab) along with the boundary conditions for the CFD simulation. For the case of the slab, the total heat flux, the driving temperature difference for the steady state heat transfer equation across the slab (return air temperature below and average plenum air temperature above) are known, along with all thermal resistances except the convective layer on top of the slab. This allows the surface convection coefficient to be calculated. The same process is used to determine the convection coefficient on the underside of the raised floor, except in this case the total heat flux is determined based on the portion of the radiant flux from the ceiling that hits the top surface of the raised floor. These convection coefficients allow the average heat flux to be calculated based on the temperature difference between the average plenum air temperature (assuming a simple well-mixed plenum and calculated as the average of all diffuser temperatures) and the average surface temperature of either of the two heat transfer surfaces: (1) underside of the floor panels, and (2) top surface of the slab. The convection coefficients are based on the detailed CFD results, but were put in these simple terms in preparation for implementation into EnergyPlus as described below. Table 1 also lists predicted temperature characteristics of the interior and perimeter zones, including the average, maximum, and minimum diffuser temperature for both zones.

The CFD results in Table 1 were reviewed to identify trends that could be included in the simplified plenum model for use in EnergyPlus. The impact of variations in plenum inlet velocity on total plenum heat gain is shown in Figure 22 for both external (Cases 1c, 1b, 2, and 3) and internal (Cases 4c, 4b, and 7) inlet locations for the fixed total airflow rate of 1 cfm/ft<sup>2</sup>. The influence of inlet velocity on total plenum heat gain was found to be relatively small for the cases investigated. A net reduction of less than 10% was observed when velocities were reduced from 1,200 fpm (6.1 m/s) down to the low value near 100 fpm (0.5 m/s) (total volume remained the same). It was only the extremely low inlet velocity of Case 3 (33 fpm) for the external inlet locations that produced a significant decrease in total plenum heat gain. For practical purposes, however, inlet velocities on the order of 100 fpm or lower would rarely, if ever, be used due to the large size of the inlet openings to deliver the required airflow into the plenum.

It is also instructive to review the temperature distributions in the interior and perimeter plenum zones for the different cases. As shown in Table 1, the uniformity of the temperature distribution in the interior and perimeter zones of the floor plate is influenced by the inlet velocities. For interior inlet locations, higher inlet velocities produce larger temperature variations within the interior zone, as some diffusers receive cool air directly from the incoming supply jet, while others receive warmer air that is recirculated back into the interior zone (e.g., Cases 4b, 4c). In the case of the very low and evenly distributed internal inlet velocities (Case 7), plenum temperature variations in the interior zone are greatly reduced, but the perimeter zone experiences much higher average temperatures. For exterior inlet locations, a similar pattern is observed, although for most simulations, the air is delivered into the plenum at a smaller angle, which tends to direct most of the cool supply air along the exterior boundary and through the perimeter zone. But in general, higher inlet velocities produce greater variations (max/min) in plenum temperatures, while the lowest inlet velocity (Case 3) produces the coolest temperatures in the perimeter zone, greater uniformity within the perimeter and interior zones, and slightly warmer average temperatures in the interior zone. While not significantly impacting total heat gain into the plenum, inlet velocities have important implications for design, control, and operating strategies.

Figure 23 shows the sensitivity of total plenum heat gain to variations in the total airflow rate for the fixed inlet velocity of 1,200 fpm. Airflow rate was varied from 0.5 to 2.0 cfm/ft<sup>2</sup> for both external (Cases 1a, 1c, 1f, and 1g) and internal (Cases 4a, 4c, 4e, and 4f) inlet locations. Total plenum heat gain demonstrates a much stronger correlation with total airflow rate compared to inlet velocity. As the total volume of air moving through the plenum increases, the average velocity of air moving within the plenum correspondingly increases, thereby impacting the average surface convective heat transfer coefficient along both the top of the slab and underside of the floor panels. Total plenum heat gain for both external and internal inlet locations followed very similar trends, increasing by 85% when airflow increased from 0.5 to 2.0 cfm/ft<sup>2</sup>.

Table 1a. Simulated Plenum Heat Gain, Convection Coefficients and Diffuser Temperature Distribution for Different Plenum Inlet Configurations: Internal inlets (Cases 1-3)

Case	Description with External Inlets	Inlet Velocity ft/min (m/s)	Heat Gain Btu/h-ft <sup>2</sup> (W/m <sup>2</sup> )	Slab Convection Coefficient Btu/h-ft <sup>2</sup> -°F (W/m <sup>2</sup> -K)	Floor Convection Coefficient Btu/h-ft <sup>2</sup> -°F (W/m <sup>2</sup> -K)	Average Perimeter Temp °F (°C)	Average Interior Temp °F (°C)	Max/Min Perimeter Temp °F (°C)	Max/Min Interior Temp °F (°C)
1a	1200 fpm 0.5 CFM/ft <sup>2</sup> Small Angle	1,200 (6.1)	3.91 (12.3)	0.43 (2.46)	0.44 (2.47)	69.5 (20.8)	69.2 (20.7)	73.6/63.9 (23.1/17.7)	73.2/66.2 (22.9/19.0)
1b	600 fpm 1 CFM/ft <sup>2</sup> Small Angle	600 (3.0)	5.36 (16.9)	0.56 (3.17)	0.56 (3.20)	66.8 (19.4)	67.3 (19.6)	70.9/62.6 (21.6/17.0)	70.2/64.1 (21.2/17.8)
1c	1200 fpm 1 CFM/ft <sup>2</sup> Small Angle	1,200 (6.1)	5.59 (17.7)	0.59 (3.36)	0.77 (4.38)	67.1 (19.5)	67.5 (19.7)	70.5/63.7 (21.4/17.6)	71.0/65.2 (21.7/18.5)
1d	1200 fpm 1 CFM/ft <sup>2</sup> Large Angle	1,200 (6.1)	5.51 (17.4)	0.57 (3.24)	0.73 (4.17)	66.8 (19.3)	67.7 (19.8)	71.5/63.2 (21.9/17.3)	69.7/64.6 (21.0/18.1)
1e	600 fpm 1.5 CFM/ft <sup>2</sup> Small Angle	600 (3.0)	6.45 (20.4)	0.67 (3.83)	0.92 (5.23)	66.0 (18.9)	66.3 (19.0)	69.7/62.5 (20.9/16.9)	67.9/63.2 (20.0/17.3)
1f	1200 fpm 1.5 CFM/ft <sup>2</sup> Small Angle	1,200 (6.1)	6.48 (20.4)	0.67 (3.80)	0.89 (5.08)	65.5 (18.6)	66.5 (19.2)	68.9/62.4 (20.5/16.9)	70.3/63.6 (21.3/17.6)
1g	1200 fpm 2 CFM/ft <sup>2</sup> Small Angle	1,200 (6.1)	7.26 (22.9)	0.86 (4.89)	1.08 (6.15)	65.3 (18.5)	65.6 (18.7)	68.3/62.3 (20.2/16.8)	68.5/62.8 (20.3/17.1)
2	Lower Velocity 1 CFM/ft <sup>2</sup>	100 (0.51)	5.08 (16.0)	0.40 (2.26)	0.59 (3.37)	65.6 (18.7)	67.8 (19.9)	71.4/62.8 (21.9/17.1)	71.6/64.6 (22.0/18.1)
3	Lowest Velocity 1 CFM/ft <sup>2</sup>	33.4 (0.17)	4.25 (13.4)	0.25 (1.41)	0.36 (2.06)	63.6 (17.6)	68.0 (20.0)	63.8/63.3 (17.7/17.4)	71.4/66.0 (21.9/18.9)

Table 1b. Simulated Plenum Heat Gain, Convection Coefficients and Diffuser Temperature Distribution for Different Plenum Inlet Configurations: External inlets (Case 4)

Case	Description with Internal Inlets	Inlet Velocity ft/min (m/s)	Heat Gain Btu/h-ft <sup>2</sup> (W/m <sup>2</sup> )	Slab Convection Coefficient Btu/h-ft <sup>2</sup> -°F (W/m <sup>2</sup> -K)	Floor Convection Coefficient Btu/h-ft <sup>2</sup> -°F (W/m <sup>2</sup> -K)	Average Perimeter Temp °F (°C)	Average Interior Temp °F (°C)	Max/Min Perimeter Temp °F (°C)	Max/Min Interior Temp °F (°C)
4a	1200 fpm 0.5 CFM/ft <sup>2</sup>	1,200 (6.1)	3.67 (11.6)	0.34 (1.93)	0.35 (1.99)	69.0/66.5 (20.5/19.2)	68.6/67.9 (20.4/20.0)	73.6/66.5 (23.1/19.2)	72.7/62.4 (22.6/16.9)
4b	600 fpm 1 CFM/ft <sup>2</sup>	600 (3.0)	5.03 (15.9)	0.45 (2.57)	0.47 (2.67)	65.4 (18.6)	68.1 (20.1)	67.1/63.5 (19.5/17.5)	72.8/62.9 (22.7/17.1)
4c	1200 fpm 1 CFM/ft <sup>2</sup>	1,200 (6.1)	5.25 (16.6)	0.50 (2.82)	0.58 (3.30)	66.8 (19.3)	67.3 (19.6)	69.4/64.7 (20.8/18.2)	71.5/63.4 (21.9/17.5)
4d	600 fpm 1.5 CFM/ft <sup>2</sup>	600 (3.0)	6.05 (19.1)	0.54 (3.09)	0.69 (3.89)	64.8 (18.2)	66.8 (19.3)	66.8/63.4 (19.4/17.4)	69.6/62.7 (20.9/17.1)
4e	1200 fpm 1.5 CFM/ft <sup>2</sup>	1,200 (6.1)	6.14 (19.4)	0.57 (3.25)	0.70 (3.96)	64.9 (18.3)	66.6 (19.2)	67.1/63.1 (19.5/17.3)	71.0/63.1 (21.7/17.3)
4f	1200 fpm 2 CFM/ft <sup>2</sup>	1,200 (6.1)	6.80 (21.4)	0.65 (3.67)	0.83 (4.73)	64.2 (17.9)	66.0 (18.9)	66.1/62.9 (18.9/17.2)	69.7/62.1 (21.0/16.7)
4g	1200 fpm 1 CFM/ft <sup>2</sup> Inlet Temp=67°F	1,200 (6.1)	3.69 (11.6)	0.48 (2.71)	0.57 (3.26)	70.3 (21.3)	70.7 (21.5)	72.1/68.9 (22.3/20.5)	73.6/67.9 (23.1/19.9)
4h	1200 fpm 1 CFM/ft <sup>2</sup> Inlet Temp=57°F	1,200 (6.1)	6.83 (21.6)	0.51 (2.91)	0.58 (3.28)	63.2 (17.3)	63.9 (17.7)	66.7/60.5 (19.3/15.8)	69.4/59.0 (20.8/15.0)
4i	1200 fpm 1 CFM/ft <sup>2</sup> Ceil Temp=73°F	1,200 (6.1)	4.46 (14.1)	0.46 (2.63)	0.61 (3.45)	66.0 (18.9)	66.5 (19.2)	68.2/64.3 (20.1/18.0)	69.9/63.1 (21.1/17.3)
4j	1200 fpm 1 CFM/ft <sup>2</sup> Ceil Temp=83°F	1,200 (6.1)	6.05 (19.1)	0.54 (3.07)	0.57 (3.22)	67.5 (19.7)	68.1 (20.1)	70.5/65.1 (21.4/18.4)	73.0/63.7 (22.8/17.6)
4k	1200 fpm 1 CFM/ft <sup>2</sup> RAT = 75°F	1,200 (6.1)	4.46 (14.1)	0.54 (3.07)	0.58 (3.30)	66.0 (18.9)	66.5 (19.2)	68.2/64.3 (20.1/18.0)	70.2/63.2 (21.2/17.3)
4l	1200 fpm 1 CFM/ft <sup>2</sup> RAT = 85°F	1,200 (6.1)	6.06 (19.1)	0.49 (2.77)	0.61 (3.46)	67.5 (19.7)	68.1 (20.1)	70.6/65.1 (21.4/18.4)	72.8/63.7 (22.7/17.6)

Table 1c. Simulated Plenum Heat Gain, Convection Coefficients and Diffuser Temperature Distribution for Different Plenum Inlet Configurations: Internal inlets and special shapes (Cases 5-9)

Case	Description	Inlet Velocity ft/min (m/s)	Heat Gain Btu/h-ft <sup>2</sup> (W/m <sup>2</sup> )	Slab Convection Coefficient Btu/h-ft <sup>2</sup> -°F (W/m <sup>2</sup> -K)	Floor Convection Coefficient Btu/h-ft <sup>2</sup> -°F (W/m <sup>2</sup> -K)	Average Perimeter Temp °F (°C)	Average Interior Temp °F (°C)	Max/Min Perimeter Temp °F (°C)	Max/Min Interior Temp °F (°C)
5	Internal Inlets 1200 fpm 1 CFM/ft <sup>2</sup>	1,200 (6.1)	5.19 (16.4)	0.50 (2.84)	0.50 (2.86)	66.9 (19.4)	66.8 (19.3)	68.5/63.1 (20.3/17.3)	68.8/66.3 (20.4/19.0)
6	Internal Inlets 1200 fpm 1 CFM/ft <sup>2</sup>	1,200 (6.1)	5.68 (17.9)	0.61 (3.49)	0.92 (5.22)	66.7 (19.3)	68.0 (20.0)	74.1/62.7 (23.4/17.0)	72.4/62.4 (22.5/16.9)
7	Internal Inlets Low Velocity 1 CFM/ft <sup>2</sup>	97.2 (0.49)	4.82 (15.2)	0.36 (2.03)	0.48 (2.71)	69.0 (20.6)	64.4 (18.0)	72.4/66.1 (22.5/19.0)	67.2/62.7 (19.6/17.0)
8a	Special Shape 600 fpm 1 CFM/ft <sup>2</sup>	600 (3.0)	5.25 (16.6)	0.45 (2.55)	0.59 (3.35)	65.1 (18.4)	68.1 (20.0)	(69.0/62.6) (20.5/17.0)	71.6/64.6 (22.0/18.1)
8b	Special Shape 1200 fpm 1 CFM/ft <sup>2</sup>	1,200 (6.1)	5.42 (17.1)	0.49 (2.79)	0.76 (4.33)	65.0 (18.3)	68.6 (20.3)	67.4/63.0 (19.7/17.2)	72.6/64.9 (22.6/18.3)
9a	Special Shape 600 fpm 1 CFM/ft <sup>2</sup>	600 (3.0)	5.42 (17.1)	0.49 (2.81)	0.68 (3.86)	66.6 (19.2)	67.3 (19.6)	71.9/62.4 (22.1/16.9)	72.4/62.9 (22.5/17.2)
9b	Special Shape 1200 fpm 1 CFM/ft <sup>2</sup>	1,200 (6.1)	5.62 (17.7)	0.57 (3.21)	0.87 (4.94)	66.5 (19.2)	67.8 (19.9)	72.6/62.8 (22.6/17.1)	73.0/63.9 (22.8/17.7)

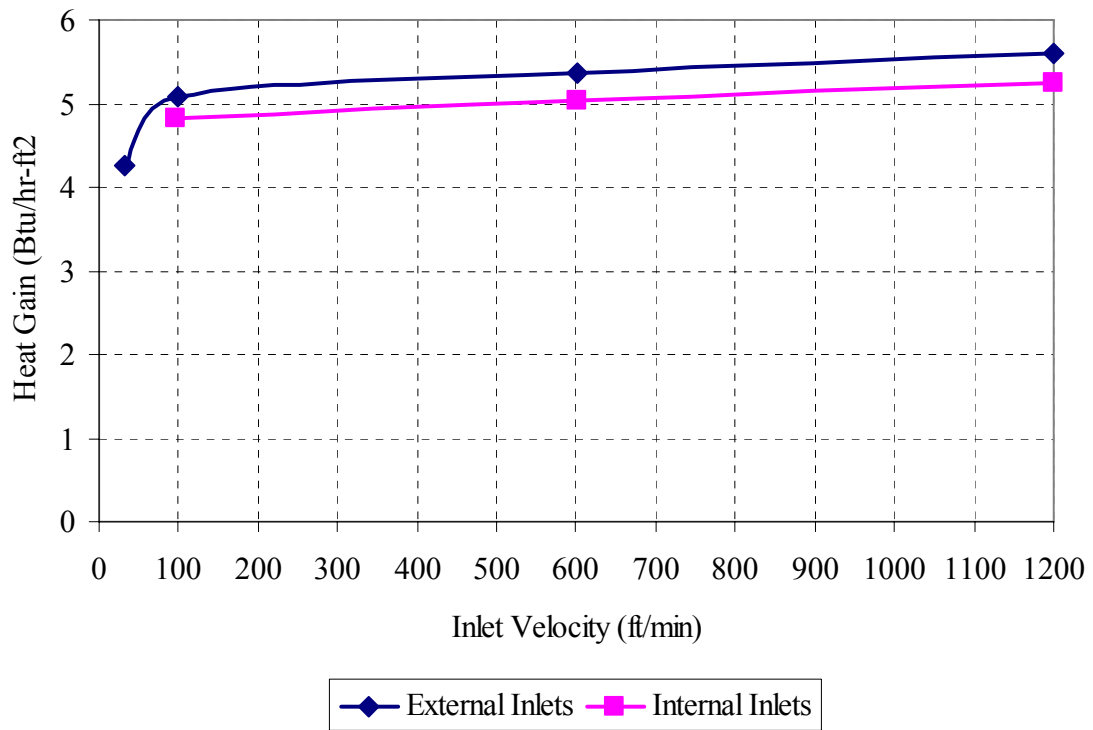


Figure 22. Sensitivity of total plenum heat gain to the inlet velocity (airflow rate=1 cfm/ft<sup>2</sup>)

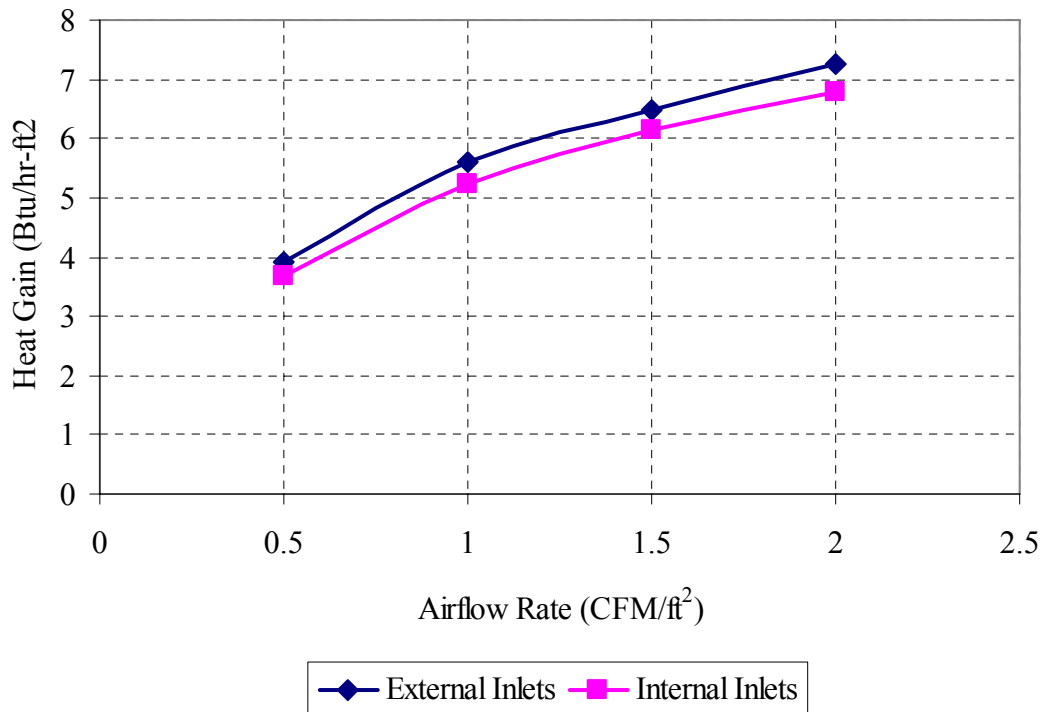


Figure 23. Sensitivity of total plenum heat gain to total airflow rate (inlet velocity=1,200 fpm)

Figures 24 and 25 present another way to compare the relative sensitivity of total plenum heat gain to variations in both inlet velocity and total airflow rate for external and internal inlets, respectively. Category labels on the x-axis combine inlet velocity with airflow rate for different cases listed in Table 1. For example, in Figure 24, “1200\_1” represents Case 1c (external inlets with small angles) with an inlet velocity of 1,200 fpm and a total airflow rate of 1 cfm/ft<sup>2</sup>. In Figure 25, “1200\_1” represents Case 4c (internal inlets) with an inlet velocity of 1,200 fpm and a total airflow rate of 1 cfm/ft<sup>2</sup>. The bar graphs clearly demonstrate the trend of increasing heat gain with increasing total airflow rate, while in contrast, changes in inlet velocity for a constant total airflow rate produce little, if any, changes in heat gain. As a result, we conclude that inlet velocity variations over typical ranges will have a small impact.

Table 1 also presents the results for Cases 4g and 4h, investigating the impact of using a higher or lower plenum inlet temperature. When compared to Case 4c, which used the default plenum inlet temperature of 62°F, we see that there is a large difference in heat gain to the plenum due to the change in temperature difference across the slab and floor panels. However, the calculated average convection coefficients on both the slab and underside of the floor show very little variation at all compared to Case 4c. Since our anticipated simplified plenum model for implementation in EnergyPlus will be based on the specification of these two key average surface convection coefficients we conclude that changes in the plenum inlet temperature have a very small impact and can be ignored in the model.

The CFD results for variations in ceiling temperature (Cases 4i and 4j) and variations in return air temperature on the floor below (Cases 4k and 4l) demonstrate relatively modest impacts on the predicted surface convection coefficients, similar to the results described above for plenum inlet temperature. These findings provide justification for the decision to base the simplified plenum model on variations in total airflow for the expected range of most practical UFAD applications.

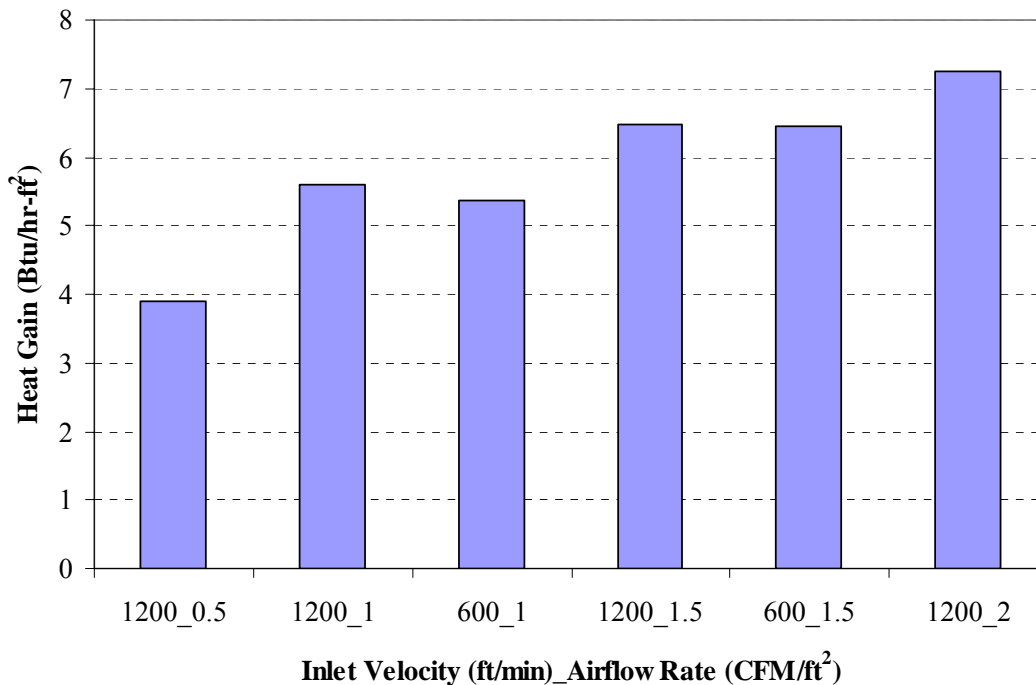


Figure 24. Sensitivity of total plenum heat gain to inlet velocity and airflow rate (external inlets)

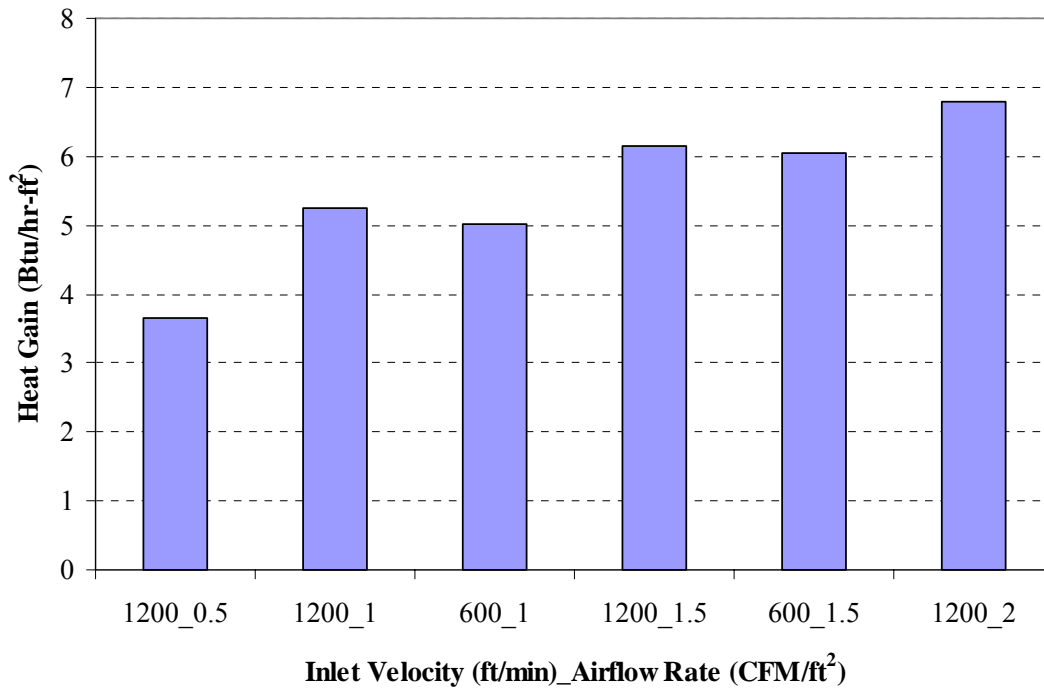


Figure 25. Sensitivity of total plenum heat gain to inlet velocity and airflow rate (internal inlets)

### 3.3 UNDERFLOOR PLENUM MODEL FOR ENERGYPLUS

Figure 26 presents a schematic diagram of how the simplified plenum model can be configured within EnergyPlus. Conditioned air from the air handler enters the underfloor plenum (Plenum 1) at the desired flow rate and plenum inlet temperature ( $T_{in1}$ ). Similar to other conditioned zones, EnergyPlus performs an energy balance on the plenum, producing a single well-mixed temperature ( $T_{plenum1}$ ). To calculate the energy balance, recommended surface convection coefficients, described below, are specified for the slab ( $h_{s1}$ ) and raised floor ( $h_{f1}$ ). The well-mixed plenum temperature ( $T_{plenum1}$ ) serves as the average diffuser discharge air temperature ( $T_{out1}$ ) entering the conditioned space (Zone 1). Note that more than one thermal zone can be served by a single underfloor plenum, and in fact, unless the user has more detailed information about the expected temperature distribution in the underfloor plenum across the entire floor plate, this is the preferred plenum configuration (one single underfloor plenum) for each floor of the building. However, if desired, one or more additional plenum zones may be added in series to the first plenum zone. In this case, as shown in Figure 26,  $T_{out1}$  is equal to the plenum inlet temperature ( $T_{in2}$ ) for the second plenum zone (Plenum 2). This permits the possibility of simulating an interior plenum zone with a cooler supply air temperature and a perimeter plenum zone with a warmer supply air temperature due to thermal decay in the plenum. Note that in this case, the airflow entering the second plenum will be reduced by the volume of air delivered into Zone 1. Due to the complexity of most underfloor plenum airflow and temperature distributions (see Table 1), until more guidance is available, it is recommended that the user specify a single underfloor plenum per floor

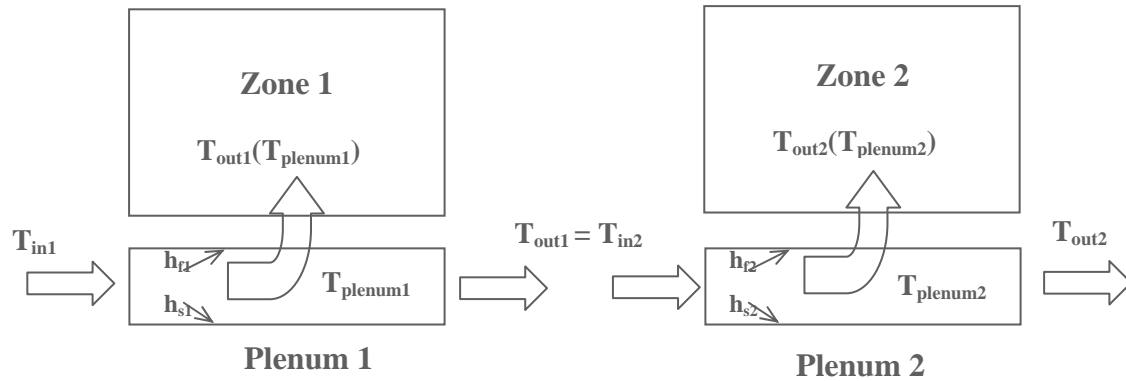


Figure 26. Schematic diagram of EnergyPlus plenum model structure

As described above, the CFD sensitivity study demonstrated that total airflow rate through the plenum was the primary factor in determining the surface convection coefficients on the top of the slab and the underside of the raised floor panels. Since convection coefficients can be easily specified within EnergyPlus, it was decided to have the simplified plenum model consist of a description of the expected average convection coefficient values for these two surfaces as a function of total airflow rate. We plotted the relationship between airflow rate and convection coefficient based on the CFD simulation results for external inlets and internal inlets in Figures 27 and 28, respectively. Also shown on the figures are polynomial fits to the predicted values for the range of airflow rates covered (0.5 – 2.0 cfm/ft<sup>2</sup>).

The following observations can be made about the results shown in Figures 27 and 28.

- The predicted surface convection coefficients are strongly correlated with total airflow rate and increase by a factor of nearly two or more over the range of airflows investigated.
- The predicted average convection coefficients for the underside of the raised floor (“floor”) are always higher than those for the top of the slab (“slab”), except at the lowest airflow rate. This is due to the fabrication of the raised floor panels which produces greater roughness and increased surface area on the underside.
- In general, the predicted convection coefficients are slightly larger for the external inlet locations (Figure 27) compared to the predictions for the same airflow rates for internal inlet locations (Figure 28). We reviewed the cause of this shift in predicted values and believe that it is driven by the tendency for most external plenum inlets to direct the supply air at a relatively small angle with respect to the external boundaries of the plenum. When the air is flowing parallel to and next to a boundary, it tends to be accelerated, thereby increasing the average air velocity within the plenum.

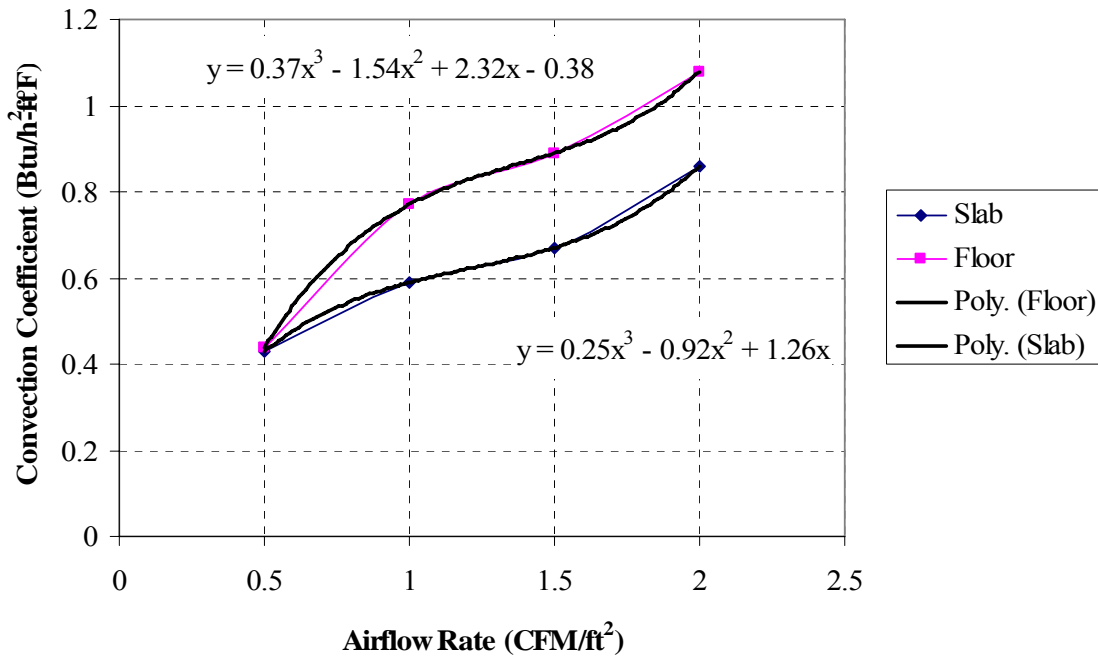


Figure 27. Average convection coefficients as a function of total airflow rate (external inlets, inlet velocity=1,200 fpm)

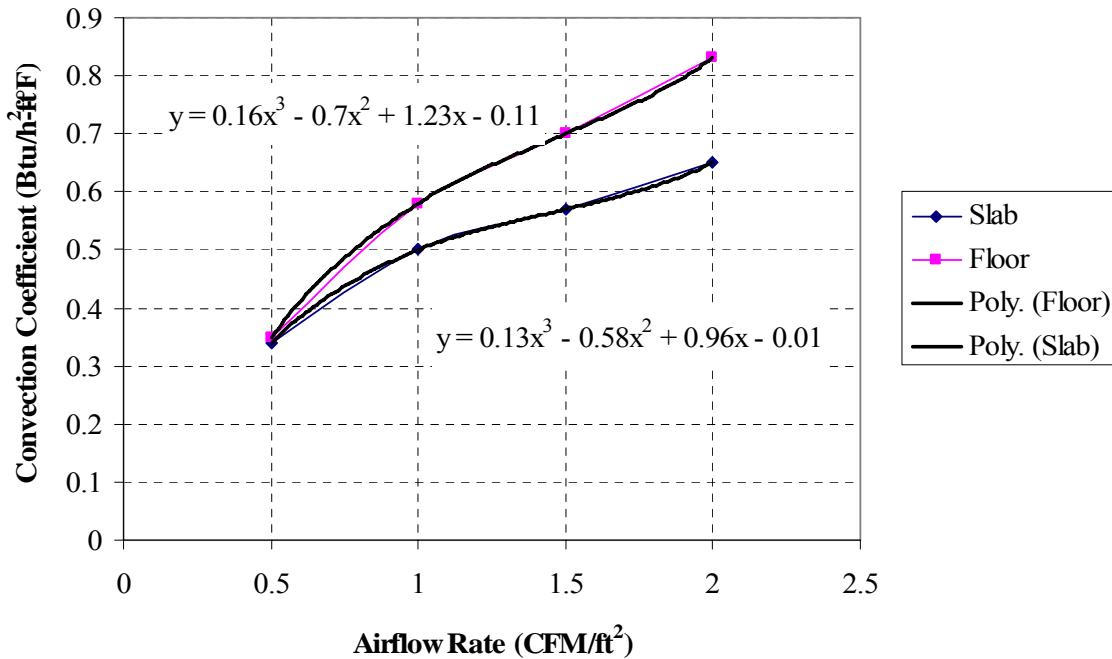


Figure 28. Average convection coefficients as a function of total airflow rate (internal inlets, inlet velocity=1,200 fpm)

In practice, although plenum inlet configurations can vary significantly from building to building, it is most common for the plenum inlets to deliver the air out into the plenum zone without being directed along a vertical side wall of the plenum. This most closely resembles the internal plenum inlet configurations simulated in Figure 28. It was therefore decided to specify the underfloor plenum model for use in EnergyPlus based on the results for internal inlet locations.

In the new version of EnergyPlus/UFAD, the underfloor plenum is modeled as a well-mixed zone (single average temperature) that exchanges heat with all surfaces in contact with the plenum air. By far the largest surfaces that transfer energy into or out of the plenum are the slab (or structural layer between floors of a building) and raised floor panels. As described in the section above, the average convection coefficients assigned to these surfaces are calculated to predict the average heat flux based on the temperature difference between the average plenum air temperature (assuming a well mixed plenum zone) and the average surface temperature of either heat transfer surface. The final specification of the underfloor plenum model consists of Equations (1) and (2), as listed below, one for the top surface of the slab and one for the underside surface of the raised floor panels.

Bottom surface of underfloor plenum zone (top surface of slab):

$$h_{slab} = 0.1333 \dot{Q}^3 - 0.58 \dot{Q}^2 + 0.9567 \dot{Q} - 0.01 \quad (1)$$

Top surface of underfloor plenum zone (underside surface of raised floor panels):

$$h_{floor} = 0.16 \dot{Q}^3 - 0.7 \dot{Q}^2 + 1.23 \dot{Q} - 0.11 \quad (2)$$

where:

$$h_{slab} = \text{average convection coefficient for top surface of slab (Btu/hr-ft}^2\text{-}^\circ\text{F)}$$

$$h_{floor} = \text{average convection coefficient for underside of raised floor panels (Btu/hr-ft}^2\text{-}^\circ\text{F)}$$

$$\dot{Q} = \text{total airflow rate entering underfloor plenum zone (cfm/ft}^2\text{)}$$

It is recognized that the above equations represent a very simplified and approximate model of a very complex airflow configuration resulting in heat exchange with the top and bottom surfaces of an underfloor plenum. Furthermore, it is recognized that underfloor plenum designs will rarely, if ever, conform exactly to the geometric and airflow assumptions upon which this model is based. However, we believe that in the majority of EnergyPlus simulations, the overall energy balance of an underfloor plenum will be relatively insensitive to all parameters except the total rate of airflow entering the underfloor plenum. This, of course, assumes that the building geometry, all materials, and all boundary conditions are accurately described in EnergyPlus. The user should be aware that there may be cases where the use of different convection coefficients may be warranted, if justified. However, we believe that in the majority of EnergyPlus simulations, the overall energy balance of an underfloor plenum will demonstrate reasonable agreement with the predictions of this simplified model. Clearly, further research may provide updated information on this topic in the future.

## 4 REFERENCES

---

- Bauman, F. 2003. *Underfloor Air Distribution (UFAD) Design Guide*. Atlanta: ASHRAE, American Society of Heating, Refrigerating, and Air-Conditioning Engineers, Inc.
- Bauman, F., H. Jin and T. Webster. 2006. Heat Transfer Pathways in Underfloor Air Distribution (UFAD) Systems. *ASHRAE Transactions*, Vol. 112, Part 2.
- Fujita, H. and S. Tomiie. 1999. Thermal Storage With Concrete Slab Of Pressurized Plenum In Underfloor Air Distribution System. *Proceedings of Building Simulation '99*, Volume 1: 499-506, Kyoto, Japan, 13-15 September.
- Jin, H., F. Bauman, and T. Webster. 2005. "Testing and Computational Fluid Dynamics (CFD) Modeling of Underfloor Air Supply Plenums." Internal Report, Center for the Built Environment (CBE), University of California, Berkeley, October.
- Jin, H., F. Bauman, and T. Webster. 2006. "Testing and Modeling of Underfloor Air Supply Plenums." *ASHRAE Transactions*, Vol. 112, Part 2.
- Launder, B. E. and D. B. Spalding. 1974. The numerical computation of turbulent flows. *Computer Methods in Applied Mechanics and Energy*. 3: 269-289.
- Nagase, O., et al. 1995. Effects of Internal Load, Supply Air Volume, and Floor Surface Conditions on the Thermal Environment in the Office Space with Underfloor HVAC. *Proceedings, Annual Conference of the Society of Heating, Air-Conditioning, and Sanitary Engineers of Japan*, Hiroshima, Japan, 2-4 October.